Revision 1

Quantitative models linking igneous amphibole composition with magma Cl and OH content

Paul A. Giesting* and Justin Filiberto

Department of Geology, Southern Illinois University, Carbondale, Illinois 62901, USA

* - Corresponding author (giesting@alumni.nd.edu)

Abstract. Minerals of the amphibole group are found in igneous rocks on Earth and other rocky bodies. Since the O(3) site of amphibole can contain OH, O^{2-}, F, and Cl, amphibole composition provides important information about water and halogen contents, oxidation state, and other features of its formation and alteration environments. However, the complexity of amphibole crystal chemistry means this information is difficult to extract. Further, it has been regular practice in the era of the electron microprobe to neglect H and Fe^{3+} analyses for amphibole, critically reducing the amount of information available in amphibole analyses in the literature.

We have assembled models and insights from previous work in order to create a methodology that allows the estimation of magmatic H_2O and Cl contents from existing amphibole analyses. Since the methodology requires use of a cation norm, we begin with a deeper investigation of the consequences of different cation normalization schemes for amphibole analyses, and provide grounds for deciding which scheme best fits a given amphibole analysis. We then show how the existing model of Popp and coworkers can be reversed to estimate the OH and $^{[O(3)]}O^{2-}$ contents of amphiboles in synthesis experiments. Using a synthetic

dataset collected from the literature (39 amphibole analyses), we calibrate a partitioning model for the OH/Cl competition on the O(3) site of igneous amphiboles:

$$K_{Cl} = (X_{Cl}/X_{OH})_{amphibole} / ([Cl]/[OH])_{melt}$$

$$\ln K_{Cl} = 6.59\ K / (Na + {}^{[A]}[\ ]) - 0.679\ Mg + 0.487\ {}^{[6]}Fe$$

where X signifies a mole fraction of an anion on the O(3) site; [Cl] and [OH] signify melt mole fractions of the anion in question on a one-oxygen (Stolper-Zhang) basis; K, Na, $^{[A]}[\ ]$, Mg, and $^{[6]}$Fe signify the amount of each component in the amphibole in atoms per amphibole formula unit, with $^{[A]}[\ ]$ denoting vacancies on the amphibole A site.

We then combine the Popp et al. model with our new model to link the occupancy of the amphibole O(3) site and other crystal chemical parameters to the Cl and H_2O content of melts crystallizing amphibole. The competition between OH and Cl for this site can be used to calculate the melt and amphibole OH/H_2O contents, as well as the speciation of Fe in amphibole, provided that the Cl content of both the amphibole and its coexisting melt is known, without analyzing either phase for H or Fe^{3+}/Fe^{2+}.

While the models in this paper should be recalibrated using future experimental data, this work shows that considerably more information about the volatile contents of magmas can be gleaned from amphibole than previously shown, and also provides additional information about the crystal chemistry of amphibole and how it affects Cl partitioning into minerals of this group.

Keywords: amphibole, mineral/melt partitioning, chlorine, water, igneous petrology

1. Introduction. Amphibole, apatite, and mica are common minerals well-suited to estimating the water and halogen content of melts (Zhang et al., 2012) or fluids (Zhu and Sverjensky, 1991).

The population of the monovalent anion site of these minerals preserves a record of their formation environment. This information is valuable in a wide range of applications from economic geology (Rasmussen and Mortensen, 2013; Smith, 2007) to planetary petrology (Boyce et al., 2010; Filiberto and Treiman, 2009a; Filiberto and Treiman, 2009b; McCanta et al., 2008; Patiño Douce et al., 2011).

Amphiboles have a particularly complex crystal chemistry (Hawthorne and Oberti, 2007a; Hawthorne and Oberti, 2007b; Hawthorne et al., 2012), which makes them valuable as indicators of a wide variety of chemical processes (Chambefort et al., 2013; Chambers and Kohn, 2012; Humphreys et al., 2009; Ridolfi et al., 2010) but also makes it difficult to disambiguate the effects of different processes. The O(3) site of amphiboles can contain OH, F, Cl, and O^{2-} (Hawthorne and Oberti, 2007a; Hawthorne et al., 2012). The partitioning behavior of the amphibole for these components relative to its genetic melt or fluid is a strong function of its cationic makeup.

Amphibole tends to reject Cl based on its large size relative to OH and F, like most rock-forming minerals (Zhu and Sverjensky, 1991), so high proportions of Cl on the O(3) site only occur in extremely saline hydrothermal or deuteric environments (Enami et al., 1992; Morrison, 1991). Cl incorporation into amphibole is encouraged by substitution of Fe for Mg on the octahedral sites, A site occupancy by K, and substitution of Al for Si on the tetrahedral sites (Enami et al., 1992; Oberti et al., 1993b; Sato et al., 2005); this is due to both a tendency toward Fe-Cl bonds and away from Mg-Cl bonds, and the expansionary effect all these substitutions have on the amphibole lattice. In contrast, amphibole readily accepts F on the O(3) site as a substitute for OH (Zhu and Sverjensky, 1991). Substitution of F can stabilize amphibole to higher *T* and *P* conditions that would dehydrate and destabilize OH-bearing amphibole (Garcia et

al., 1980; Holloway and Ford, 1975; Johnson and Fegley, 2003).

O^{2-} on the O(3) site, or oxo-component (Hawthorne and Oberti, 2007ab; Hawthorne et al., 2012) is widely known in calcic, titanian amphiboles of igneous rather than metamorphic origin (Martin, 2007; Schumacher, 2007). This substitution increases negative charge and must be counterbalanced by one of the many possible cation substitutions that would also increase charge. The two most important cations substituted in are Ti^{4+} and Fe^{3+}, with Al^{3+} also of importance (King et al., 1999, 2000; Popp et al., 2006). Amphiboles are susceptible to the internal reaction

(1) $Fe^{2+} + OH^- \rightarrow Fe^{3+} + O^{2-} + 1/2\ H_2$

whereby iron oxidation is coupled to dehydrogenation (Demeny et al., 2006; Dyar et al., 1993; Dyar et al., 1992; King et al., 1999; Martin, 2007; Popp and Bryndzia, 1992; Popp et al., 1995, 2006). This dehydrogenation reaction can occur at subsolidus conditions, which can interfere with attempts to use amphibole compositions to determine water contents of source magmas (Lamb and Popp, 2009); further, it may occur in the forward or reverse direction as a result of shock (Minitti et al., 2008ab), adding uncertainty to attempts to use amphibole compositions from meteorites to constrain the properties of source magmas on extraterrestrial bodies.

Goals. In this work, we reconsider the methodologies used to calculate amphibole formulae from chemical composition data (Hawthorne and Oberti, 2007a; Leake et al., 1997; Schumacher, 2007) and suggest revised tests to determine which methodology is most appropriate for different amphiboles with differing amounts of available chemical information.

We then consider an existing model of amphibole chemistry (Popp et al., 1995, 2006) and show how it can be used in an inverse sense: instead of estimating H_2O activity and fugacity in the source region of the amphibole based on the H content of the amphibole, if the H_2O activity of the source melt is known or estimated, the model can be used to calculated the amount of OH and O^{2-} on the O(3) site.

Next, we use this methodology to recalibrate the model of Sato et al. (2005), using the calculated OH abundance instead of assuming 2 = OH + F + Cl, and incorporating additional synthetic data (Adam and Green, 1994, 2006; Adam et al., 2007; Hauri et al., 2006; McCubbin et al., 2008).

Finally, we show how using both models together generates enough constraining equations to result in a determined system for situations where the *P, T, f*(O_2) of formation, the melt Cl composition, and a typical amphibole composition by electron microprobe (EMP) are available. With this coupled model system of equations, the H_2O content of both amphibole and melt, along with the Fe^{3+}/Fe^{2+} ratio of the amphibole can be calculated: a powerful method to extend the utility of conventional EMP analyses, and a way of checking, in the case of potentially disturbed systems with H contents determined by, e.g., ion microprobe, whether the amphibole and/or melt have lost H since the Cl equilibrium state was set.

At present, we must assume that the Popp et al. (2006) model is extensible to amphiboles beyond the pargasite and kaersutite compositions they used to calibrate it. We do not have enough experimental data at present to recalibrate this model, and we do not have any means of quantifying the error in so extending it. We provide error estimates for our model parameters, but these calculated errors only describe how well the Cl/OH partitioning model equation predicts the Cl/OH partitioning coefficients in our calibration dataset, as opposed to the unknown

116 error in the calculated OH and $^{[O(3)]}O^{2-}$ content of the calibration amphiboles. This paper shows
117 the methodology and its benefits: in particular, use of the Popp et al. (2006) model to calculate
118 OH and $^{[O(3)]}O^{2-}$ allows much better fitting of the data of Sato et al. (2005) than they were able to
119 achieve without it. The model equations presented here are not, however, to be regarded as
120 settled.
121
122 **2. Calculation of amphibole formulae**. Calculation of amphibole formulae from electron
123 microprobe or other chemical data is often a vexing process. It is commonly assumed that OH +
124 F + Cl sum to 2.0 apfu (atoms per formula unit), which allows a normalization to the anhydrous,
125 halogen free basis of 23 O (Leake et al., 1997) but this assumption is not generally true,
126 especially for igneous amphiboles (e.g. kaersutites and "basaltic hornblendes"), which are known
127 to contain considerable O^{2-} on this site (Deer et al., 1997; Dyar et al., 1992, 1993; Hawthorne and
128 Oberti, 2007a; King et al., 1999; Leake et al., 1997; Martin, 2007; Popp and Bryndzia, 1992;
129 Popp et al., 1995, 2006). Normalization schemes to 23 O are discussed in detail by Leake et al.
130 (1997) and Schumacher (2007). These authors propose calculating two normalizations, one
131 assuming all Fe is Fe^{2+}, the other assuming all Fe is Fe^{3+}, comparing the results to an extensive
132 list of "chemical" and "stoichiometric" limits, using these to calculate adjusted minimum and
133 maximum permissible values for ferrous and ferric iron, and then generally taking the mean
134 between these values as the determined speciation of iron in the amphibole. This complex
135 process is by no means always used in the literature, and its results are not particularly
136 satisfactory, although they are better than the default assumption of all Fe being Fe^{2+} or Fe^{3+}
137 (Hawthorne and Oberti, 2007a).
138 Instead, many studies use one of a few cation normalization schemes. Amphibole group

minerals contain twenty-four anions and between fifteen and sixteen cations per formula unit. The cations sit on at least seven crystallographically distinct sites, one of which can be vacant, partly, or totally filled. These seven crystallographic sites can be grouped into four distinct size and coordination types: in order of increasing size, two tetrahedral/4-fold coordination sites, three octahedral/6-fold coordination sites, an 8-fold or 6+2 fold or even 4+4 fold (Oberti et al., 1993a) coordinated site, and the large potentially vacant A site (Figure 1). These four site types can be occupied by all the common cations in silicates (Hawthorne and Oberti, 2007a). Common major element constituents of amphiboles are located as follows:

- The tetrahedral sites are occupied by Si and Al (much less commonly Ti; Leake et al., 1997).
- The octahedral sites are occupied by Al, Ti, Cr, Mg, Mn, Fe^{2+} and Fe^{3+}.
- The 8-fold sites are occupied by Mg, Mn, Fe^{2+}, Ca, and Na.
- The large A sites are vacant or occupied by Na, K, and very rarely Ca (Leake et al., 1997).

A given cation is commonly found on more than one type of site in a given amphibole. The most common overlap situations involve Al on both tetrahedral and octahedral sites; Mg, Fe^{2+}, and Mn on both octahedral and 8-fold sites; and Na on both 8-fold and A sites. Ti occupancy of tetrahedral sites and Ca occupancy of the A site are rare and appear to be limited to peculiar chemical environments (Hawthorne et al., 1996a; Hawthorne et al., 1996b; Leake et al., 1997). The likelihood of vacancies and the amount of overlap that can occur between sites are troublesome for any method of cation normalization; nevertheless, since it obviates the need to determine Fe^{2+}/Fe^{3+} and volatile constituents, cation normalization is commonly used.

Probably the two most common cation normalization schemes for amphiboles are, in this

order, the 13-cation scheme, where all cations outside of Ca, Na, and K are assumed to occupy and fill the tetrahedral and octahedral sites, and the 15-cation scheme, where all cations outside Na and K are assumed to occupy and fill the non-A cation sites (Hawthorne and Oberti, 2007a). These schemes are directed specifically at calcic amphiboles (e.g. hornblende, actinolite, pargasite, edenite), in which Ca dominates the 8-fold site. The 15-cation scheme is also applicable to ferromagnesian amphiboles in which Fe and Mg dominate the 8-fold site. The 13-cation scheme is also applicable to sodic amphiboles, in which Na occupies a large fraction of the 8-fold site.

Igneous amphiboles in mafic to intermediate rocks are generally calcic (Deer et al., 1997; Hawthorne et al., 2012), although exceptions are known (e.g., Shane et al., 2007). The twofold defining assumption of the 13-cation scheme implies that significant Fe does not occupy the 8-fold site and significant Ca does not occupy the octahedral site. If this assumption is not true, the 13-cation scheme will underestimate the number of cations in the overall amphibole formula. The 15-cation scheme assumes that Ca does not occupy the A site and Na does not occupy the 8-fold site; if this assumption is invalid, the 15-cation scheme will produce an excess of cations in the calculated formula.

There are solvus relationships between the calcic amphiboles and the Mg-Fe amphiboles, as well as between the calcic amphiboles and the sodic amphiboles. In natural systems, these cause exsolution of high-temperature (and/or high-pressure) binary or ternary amphiboles into two or three phases of more dominantly calcic, sodic, or ferromagnesian affinity (Smelik and Veblen, 1992a, 1992b, 1993, 1994). Unexsolved amphiboles generally have >1.5 apfu of the dominant cation on the 8-fold site (e.g. tremolites on the glaucophane-tremolite solvus synthesized by Jenkins, 2011 with 1.6-1.65 apfu $^{[8]}$Ca), making both the 13-cation and 15-cation

schemes at least crudely applicable to any calcic amphibole. Zingg (1996) noted that in the rock suites he studied, Na appeared to be accommodated in calcic amphiboles dominantly by the edenite exchange, i.e., a substitution from a low-alkali, A-site vacant base composition via the exchange vector $^{A}(Na,K)_1{}^{[4]}Al_1{}^{[4]}Si_{-1}$, with the glaucophane exchange ($^{[8]}Na_1{}^{[6]}Al_1{}^{[8]}Ca_{-1}{}^{[6]}Mg_{-1}$) of marginal importance, while the cummingtonite exchange ($^{[8]}Fe_1{}^{[8]}Ca_{-1}$) was more evident; thus, for the amphiboles in his study, the 15-cation normalization would provide significantly more accurate results than the 13-cation scheme.

A third cation normalization scheme, the 16-cation normalization, assumes full occupancy of the cation sites in the amphibole (Hawthorne and Oberti, 2007a). This can be a relatively accurate assumption for certain amphiboles. It is well-known that Na and K occupation of the A site is positively correlated with temperature (Holland and Blundy, 1994). While pressure effects on A site occupancy are seldom discussed in the literature, it seems clear that the edenite exchange vector above should result in substantial molar volume reduction of the amphibole+fluid or melt system, with any increase in amphibole unit cell volume more than offset by the replacement of (Na,K)+Al in the external environment with Si; therefore the edenite exchange should be expected to progress toward completion at high pressure. Thus both high *T* and high *P* conditions, in the presence of adequate alkalis and Al, should produce amphiboles that tend toward full cation site occupancy.

3. Suggested methods for normalization of igneous amphibole formulae. To use igneous amphibole compositions to study the volatile contents of their parental magmas, it is highly desirable to find a normalization scheme that does not constrain the O^{2-} content of the O(3) site to 0 (King et al., 1999; Lamb and Popp, 2009; Popp et al., 2006) or to another value such as

208 $^{[O3]}O^{2-}$ = 2 Ti (Hawthorne et al., 2012; Leake, 1968; Saxena and Ekstrom, 1970). For amphibole
209 analyses where Fe_2O_3/FeO and H_2O have not been determined, which are the vast majority of
210 those in the literature, a cation normalization procedure is the only way to accomplish this.
211 Mazdab (2003) converted the six stoichiometric checks recommended by Leake et al.
212 (1997) and others into cation normalizations, then checked the results of these normalizations for
213 charge balance and cation site type occupancy constraints. This allowed him to choose sensible
214 normalization results for at least one of the normalization types. We propose a procedure with
215 some similarities, using the three cation normalizations described above: 13-cation, 15-cation,
216 and 16-cation, and comparing their results to one another and to a 23 O anion normalization.
217 After calculating the results of all three normalizations, we bin the cations in a
218 standardized order. All Si is placed on tetrahedral sites, which are then filled with Al. Residual
219 Al is placed on the octahedral sites, followed by Ti, Mg, and Mn; the octahedral sites are then
220 filled with Fe. In reality, Fe, Mn, and Mg will all occupy the 8-fold site if any of them do, but
221 this is the simplest convention. The important distinction is between smaller divalent cations and
222 Ca on the 8-fold sites. Residual Fe is placed on the 8-fold sites, followed by Ca, with Na added
223 to fill the 8-fold sites if needed. Residual Ca, Na, and all K are placed on the A site, which may
224 be partly vacant.
225 The next step is to calculate the positive charge due to cations, with the temporary
226 assumption that all Fe is present as FeO. For a charge-balanced amphibole with no O^{2-} on the
227 O(3) site, the cations should contribute 46+ to the structure to balance the anions (22 O and 2
228 OH, F, or Cl). This is equivalent to checking how closely the normalization corresponds to a 23
229 O normalization with all ferrous iron. The results will in general not equal the ideal total of 46+.
230 To correct this, we take one of two steps depending on whether there is a deficit or an excess of

positive charge. In case of a deficit, we calculate the amount of Fe^{3+} substitution for Fe^{2+} that would be required for charge balance; in case of excess, we calculate the amount of O^{2-} substitution for OH^- that would achieve the same. This calculation can be checked by summing the anions to see if they equal the amphibole total of 24.

This procedure gives a minimum adjustment required for charge balance. It is possible to add more of both Fe^{3+} and O^{2-} (in equal amounts) to the compositions calculated this way according to equation 1 above. This does not affect the overall anion to cation ratio, since the additional anions introduced by Fe_2O_3 in place of FeO are offset by the H_2O lost by O^{2-} substitution. Thus, the maximum adjustment will be the one that either converts all Fe on the octahedral sites to Fe^{3+} or converts all OH to O^{2-}, whichever comes first. The resulting composition will still be subject to the constraints imposed by the choice of cation normalization. For ease of discussion, we define the quantity Δ_{oxo}:

(2) Cation charge (all ferrous iron) - 46 = $\Delta_{oxo} = X(^{[O(3)]}O^{2-}) - X(Fe^{3+})$

where X is the molar quantity of the component in question in apfu. Δ_{oxo} is positive when the oxo-component exceeds the amount of ferric iron in the amphibole, negative when the reverse is true.

We can reinterpret the results of a 23 O normalization with all Fe assumed to be Fe^{2+} as a normalization requiring $\Delta_{oxo} = 0$ (equal amounts of Fe^{3+} and oxo-component). We can calculate the results of a 23 O norm for comparison to the results of the cation norms with this corollary in mind to assist in choosing the best amphibole formula in a given situation.

We suggest a non-exhaustive list of checks that may allow rejection of one or more norm calculations, or will at least give more information about the consequences of choosing one scheme over another. The reader, again, should bear in mind that our focus is on igneous

amphiboles.

- Compare the values of the normalization factors for all schemes, including 23 O. Any scheme whose normalization factor exceeds the 16 cation factor is unrealistic.
- Compare Δ_{oxo} to $^{[6]}$Fe. If $-\Delta_{oxo} > {}^{[6]}$Fe, the scheme in question (probably the 13-cation scheme) is unrealistic.
- Conversely, if $\Delta_{oxo} > 2 - F - Cl$, the scheme in question is unrealistic.
- Any 13-cation or 23 O norm that requires K or vacancies ([ ]) on the 8-fold sites is also unrealistic.
- If the 13-cation norm assigns a large amount (>0.3-0.4 apfu) of Na to the 8-fold site, or if the 16-cation norm assigns significant Ca (>0.1 apfu) to the A site, the 15-cation norm is usually preferable.
- Evaluate the Δ_{oxo}/Ti ratio. Popp et al. (1995, 2006) show that this ratio is commonly equal to 1.0 for pargasites and kaersutites. Hawthorne et al. (2012) suggest a maximum of 2 for this ratio based on older work (Leake, 1968; Saxena and Ekstrom, 1970). A very large value for this ratio (>3) suggests that Δ_{oxo} is too high.

Other criteria are described in Mazdab (2003).

To illustrate this methodology, we have included Supplemental Information Table 1, which includes analyses for a variety of igneous amphiboles. The reader is invited to reuse these spreadsheets to check the results of multiple normalization schemes on their own amphibole data. Examining the results, we note several patterns:

- A typical igneous calcic amphibole will provide similar formulae when normalized to 15 cations or 23 O. A few tenths of an apfu of $^{[8]}$Fe are required in these schemes. The 13 cation scheme will replace this with $^{[8]}$Na and will usually require a minimum of ~50% of the Fe to be Fe^{3+}. For some of these amphiboles, the 13 cation scheme is untenable due to the assignation of $^{[8]}$K or $^{[8]}$[ ]. The 16 cation scheme forces a few to several tenths of an apfu of $^{[A]}$Ca and is unrealistic.
- The cummingtonite data provided by Shane et al. (2007) illustrate that the 15-cation norm and the 23 O norm are the only ones that provide reasonable results for this class of amphiboles, which have nearly vacant A sites and 8-fold sites dominated by Fe+Mg+Mn.
- The 2007 Bezymianny amphibole compositions (Turner et al., 2013) are unusual in that they have nearly equal 16-cation and 23 O normalization factors. We prefer the 15-cation normalizations for these amphiboles as well, since the 13 cation norms require nearly 100% Fe^{3+}, while the other norms demand 0.1-0.25 apfu $^{[A]}$Ca. These amphiboles have low Si, $^{[6]}$Al, and Ti relative to other amphiboles in the dataset, which may have discouraged the inclusion of $^{[O(3)]}O^{2-}$, even in an oxidizing environment enriched in Fe^{3+} (King et al. 1999; Popp et al. 2006).
- Kakanui amphibole has Na+K>1 no matter which scheme is used; the 15-cation scheme is unusable. The 13-cation and 23 O factors are close, and they calculate ~0.4 apfu $^{[8]}$Na. The 16-cation norm instead calculates ~0.15 apfu $^{[8]}$Na and ~0.2 apfu $^{[8]}$Fe, which seems equally realistic. In any case, this high *P* mineral is the only amphibole in our dataset required to have a significant glaucophane component.
- The amphiboles synthesized by Adam and Green (1994, 2006), Adam et al. (2007), and McCubbin et al. (2008) were grown at high *P* (>9 kbar) and *T* (>980 °C). These

amphiboles have very similar 15-cation and 16-cation formulae with Na+K ~ 1. As noted above, these growth conditions are expected to favor full occupancy of the amphibole structure via the edenite exchange, so these results are as expected. The 23 O formulae have 0.0-0.17 apfu $^{[8]}$Na, 0.1-0.25 apfu $^{[A]}$[ ], and are also reasonable. All three schemes yield ~0.45-0.76 apfu $^{[8]}$Fe for the McCubbin et al. (2008) synthetic amphiboles. At these conditions, the cummingtonite-hornblende solvus is likely closed (Smelik and Veblen, 1994; Zingg, 1996) and there is no reason to discredit these results. On the other hand, while the 13-cation scheme yields reasonable cation occupancies for these amphiboles, the minimum amount of Fe^{3+} they require is near or at 100% of the total iron available, which is unrealistic for amphiboles crystallized at mantle-equivalent $f(O_2)$ (King et al. 2000).

The cation normalization and follow-up procedure described only fixes minimum and maximum values of Fe^{3+} and the oxo-component of the amphibole. The traditional response to this kind of ambiguity was to take an average between the minimum and maximum possible values of $Fe^{3+}/\Sigma Fe$ (Leake et al., 1997); and in the absence of any data about the formation environment of the amphibole, this is probably the best solution (Hawthorne and Oberti, 2007a). The next section describes how we can improve on this estimation technique when information about the formation environment is available.

4. Use of $f(O_2)$ and $f(H_2O)$ to calculate redox state of amphibole. Popp et al. (1995, 2006) provide a quantitative model to evaluate the relationship between the amphibole Fe/H redox state in equation 1 and the external environment of the amphibole. For a fully characterized

amphibole, the model produces a value of $f(H_2)$ that can be combined with estimates of $f(O_2)$ to evaluate the H_2O activity or fugacity of the amphibole source region, or the conditions under which it last equilibrated. The model was calibrated using data from two pargasites and one kaersutite over the temperature range 700 - 1000 °C and pressure range 1 - 10 kbar.

In a situation where data is available for $f(H_2O)$ and $f(O_2)$, along with an ordinary suite of electron microprobe data for amphibole composition (including halogens), for example in synthesis experiments with a controlled amount of H_2O and an $f(O_2)$ buffer, we can reverse the model and use it to calculate the amount of Fe^{3+}, Fe^{2+}, $^{[O(3)]}O^{2-}$, and OH in the amphibole. This is done by starting with the equation (Popp et al., 2006)

(3) $$K_x = 28.94\, f(H_2)\, [X^2(Fe^{3+}) \cdot X^2_{oxo}] / [X^2(Fe^{2+}) \cdot X^2(OH)]$$

where X is the molar quantity of each component in the amphibole, $X_{oxo} = X(^{[O(3)]}O^{2-})$, and K_x is an effective equilibrium constant (see the original reference for further explanation). Once we have selected an amphibole normalization as discussed above, we can make substitutions like the following based on equation 2:

$$X(Fe^{3+}) = X_{oxo} - \Delta_{oxo}$$

(4) $$X(Fe^{2+}) = X_{\Sigma Fe} - X(Fe^{3+})$$

$$X(OH) = 2 - X(F) - X(Cl) - X_{oxo}$$

With these substitutions, equation 3 can be converted into a quartic polynomial equation in X_{oxo}, with all other quantities calculated from the normalized amphibole formula or the known external conditions. This equation can be solved analytically, but it is easier to use numeric methods. One root will be equal to $2\text{-}X(F)\text{-}X(Cl)$ (a trivial root, implying no OH present in the amphibole) while another (the chemically significant root) will be between this value and Δ_{oxo}.

Supplemental Table 2 shows the results of the use of this equation for the synthetic

amphiboles in Supplemental Table 1.1. For the Sato et al. (2005) data, since there are no estimates of phase proportions in their run products, their claim of water saturation in all experiments has to be accepted, and the $a(H_2O)$ of their systems is assumed to be 1.0. For the other experiments, the authors reported phase proportions, which allowed the H_2O content of their experimental melts to be compared to calculated H_2O solubility values (Moore et al., 1998); the systems were all found to be H_2O-undersaturated. We therefore calculated the $a(H_2O)$ of these systems using the model of Burnham (1997). (The interested reader may consult Appendix 1 to learn why we chose these models out of the many published models for H_2O solubility in silicate melts.) The resulting quartic equation for each analysis was solved for the appropriate root using the nonlinear, continuous GRG Solver routine in Microsoft Excel©. The results of these calculations are intuitively reasonable: most of the X_{oxo} values are only a few tenths of an apfu above the Δ_{oxo} values, and the exceptions are the three high-$f(O_2)$ runs from Sato et al. (2005). Once X_{oxo} is calculated, the Fe^{3+} content and other properties of the amphibole can be calculated from the crystal chemical constraints in equation 4.

Thus, we see that the Popp et al. (2006) model, and future refinements and extensions to it, can be used to estimate the seldom-measured H_2O and Fe_2O_3 content of amphiboles from an environment whose $f(O_2)$ and $a(H_2O)$ is sufficiently well-known or controlled. It is possible to constrain these parameters for igneous amphiboles in a more indirect, but often more readily measured, fashion, using the Cl content of equilibrated melt (preserved as quenched glass) and exploiting the competition between Cl and OH for the amphibole O(3) site. The next section will discuss this competition, while the section after will show how the Cl/OH model and the Fe/H model just described can be used in tandem to calculate the H_2O content of melts crystallizing amphibole as well as the Fe_2O_3 and H_2O content of the amphibole itself.

5. Chlorine partitioning between amphibole and melt; a recalibration of the model of Sato et al. (2005). Equilibrium partitioning behavior for many trace and minor elements or chemical components is adequately described by a bulk partition coefficient *D*:

$$D_X = C_X(\text{mineral}) / C_X(\text{melt or fluid})$$

where *C* is the weight fraction of the element or component X in the phase in question. *D* may or may not be known as a function of temperature, pressure, or chemistry of either the mineral or the melt/fluid; in many cases it is quoted as a catch-all constant (e.g. Filiberto and Treiman, 2009a; Zhang et al., 2012). Such a formulation is not adequate for H_2O, F, and Cl in amphibole at better than an order-of-magnitude level, as can be seen in Figure 2, where *D* is calculated and plotted against absolute temperature for syntheses in Supplemental Tables 1 and 2. As can be seen, D_{Cl} varies by a factor of ~5 at a given temperature and is less than 1 for all reliable analyses. This is unsurprising, given the complex crystal chemistry of amphibole and the relative misfit between Cl and the other possible occupants of the O(3) site. Further, unlike typical trace or minor constituents, the halogens and OH fulfill a critical role in crystallizing amphibole—except in the extreme case of an oxo-only amphibole, these components are required in order to occupy the O(3) site of the lattice; they are also limited to this site, and cannot occupy other sites in the lattice in any significant quantity. In this situation, the simple *D* formalism is inadequate to explain the behavior of the amphibole-melt(-fluid) system.

Zhang et al. (2012), in their assessment of currently available models for halogen partitioning between minerals and melts, cite Sato et al. (2005) as the only such model for amphibole. This model calculates a molar partitioning reaction coefficient K_{Cl}:

392 (5) $K_{Cl} = (X_{Cl}/X_{OH})_{amphibole} / ([Cl]/[OH])_{melt}$

393

394 where [] indicate mole fraction on a 1O basis (Appendix 1) as a function of the Mg# (= Mg/(Mg
395 + ΣFe)) of the amphibole and temperature *T*. This model was calibrated for synthetic hornblende
396 crystallized from water-saturated melts of Unzen rocks, or Fe-enriched Unzen rocks, at 800 to
397 850 °C and 1.85 to 3 kbar. This model is a significant advance compared to previous discussions
398 of amphibole crystal chemistry vis-a-vis chlorine partitioning (Enami et al., 1992; Morrison,
399 1991; Oberti et al., 1993b) but it is calibrated for a very narrow range of *P, T,* and chemical space
400 relative to the known stability fields of various amphiboles. It is likely not applicable to
401 petrological problems involving, e.g., basaltic melts.

402 Another potential drawback to the Sato et al. (2005) model is that it explicitly assumes 2
403 = OH + F + Cl, equivalent to a lack of oxo-component in the amphibole. As seen in
404 Supplemental Table 2, the Popp et al. (2006) model predicts significant oxo-component even
405 under conditions of water saturation ($a(H_2O) = 1$). To use the actual formulation of Sato et al.
406 (2005), one must ignore oxo-component and treat it as equivalent to OH.

407 In Supplemental Table 3, we show the results of reproducing the calculations in Table 5
408 of Sato et al. (2005) on an augmented dataset that includes amphibole and glass data from
409 basaltic, ferroan basaltic, alkali basaltic, and andesitic melts (Adam and Green, 1994, 2006;
410 Adam et al., 2007; Browne, 2005; Hauri et al., 2006; McCubbin et al., 2008), all of which were
411 crystallized at higher *T* and most of which were crystallized at higher *P* than any of the Sato et al.
412 (2005) amphiboles. The reader should note that we were unable to reproduce the Sato et al.
413 (2005) calculations even for their own syntheses, possibly because they did not cite a reference
414 for $f°(H_2O)(P,T)$. In this paper, we employ the Helmholtz energy formulation for H_2O of Pitzer

and Sterner (1994) and the fugacity equation from Sterner and Pitzer (1994). The resulting fit to Sato et al. (2005)'s original equation (Figure 3) is therefore poorer than the one reported in their paper for their own data. Still poorer is the fit to the added data, especially the very high pressure data. The poor fit to the data of Browne (2005) may be due to problems with his amphibole or glass analyses, since his synthesis conditions were quite similar to those of Sato et al. (2005). As for the rest of the added data, even with the moderate amount of systematic error introduced by changing water fugacity models, it seems clear that the Sato et al. (2005) equation is not applicable to amphiboles in basaltic or andesitic melts at ~10 kbar, ~1000 °C and above.

We recalibrated the Sato et al. (2005) partitioning model using our entire synthetic dataset, except for the Browne (2005) data, and amphibole OH contents calculated according to the methodology of the previous section of this paper, including the use of 15 (or in one case, 16) cation norms for all amphibole compositions. Most of the complexity in this calculation involves finding an appropriate value of $[OH]_{melt}$ in equation 5.

We had to make two important assumptions in order to carry out these calculations, and we considered the results of different options in each case. Our additional data were obtained from systems crystallized inside graphite capsules, rather than systems in precious metal capsules with an external metal and/or ceramic oxygen buffer as Sato et al. (2005) used. Graphite capsule systems are partially buffered by the reaction of graphite with aqueous components even in the absence of a free aqueous fluid phase (Holloway et al., 1992; Médard et al., 2008; Pilet et al., 2010; Ulmer and Luth, 1991). We therefore ran all of our calculations assuming $f(O_2)$ 0.8 log unit lower than the water-saturated GCO (graphite-carbon oxides) buffer (Médard et al., 2008; Ulmer and Luth, 1991) for the syntheses in graphite capsules. We observed little difference in the calculated K_{Cl} for higher (GCO) or lower (GCO-1) $f(O_2)$ conditions.

438 The other assumption regards the H_2O speciation model employed to determine [OH] in
439 the melt. Sato et al. (2005) used the method of Zhang (1999) for this purpose, which defines two
440 quasi-reaction constants K_1 and K_2 that, roughly speaking, govern H_2O solubility and speciation
441 in silicate melt respectively. While Sato et al. (2005) apparently used the K_1 of Zhang (1999),
442 who supplies a temperature and pressure-calibrated expression for K_1 for rhyolitic melt on the
443 basis of solubility data, they employed K_2 as determined by Nowak and Behrens (2001). Both
444 constants were determined for rhyolitic systems and are probably not ideal fits for the dacites of
445 Sato et al. (2005), let alone the more mafic systems of our auxiliary data. For the dacite dataset,
446 we substituted the K_2 of Liu et al. (2004), which is recommended by Zhang and Ni (2010).
447 Few workers calculate a K_1 as described by Zhang (1999), and there is little solubility
448 data for dacite in the literature with which to constrain K_1. Ohlhorst et al. (2001), whose primary
449 concern was synthesizing bubble-free glasses for spectroscopic calibrations, provide solubility
450 data that allow a calculation of K_1 for two samples at 1-2 kbar, 1200-1225 °C using the same
451 method Zhang (1999) employed to calibrate K_1 for rhyolite, including the use of K_2 (Liu et al.,
452 2004) to reconstruct high T speciation. These dacite K_1 values are near 9.7×10^{-6}, ~40% lower
453 than the values calculated by Zhang (1999)'s rhyolite K_1 regression (~1.3×10^{-5}). Liu et al. (2004)
454 only supply solubility data at 1 bar and ~500 °C, well out of the range in which the K_1 regression
455 is claimed accurate; 1 bar dacite K_1 values are two orders of magnitude higher than those
456 returned by the regression. We have therefore calculated total water solubility in the dacites
457 ($[H_2O]_t$) following Moore et al. (1998) instead of determining $[H_2O]_m$ and $[H_2O]_t$ via a K_1.
458 For the basaltic data, a value for K_1 was not needed since the melt was undersaturated (no
459 aqueous fluid phase was present), and by assuming an approximate amount of H_2O content of the
460 amphibole (1.1 to 1.4 wt%) one could figure the amount of H_2O in the melt by mass balance,

461 then check the accuracy of the approximated amphibole H_2O content at the end of the whole
462 calculation. We tried two formulations for speciation in the basaltic melts: the temperature-
463 independent regular solution model (Dixon et al., 1995; Silver and Stolper, 1989), and K_2
464 expressions temperature calibrated by means of glass transition theory (Lesne et al., 2011). The
465 regular solution model yields an equation that must be solved numerically to determine
466 speciation. The results of the temperature-independent calculation are a higher $[H_2O]_m$ and a
467 lower [OH] compared to the K_2 calculation for the melts in question, and we tried regression
468 against both sets of results.

469 We employed standard multiple linear regression techniques (Iman, 1994) in Microsoft
470 Excel© on a chosen family of 19 crystal chemical and environmental parameters to determine
471 which were most significantly correlated with our redetermined values of ln K_{Cl}. Our procedure
472 is discussed in more detail in Appendix 2. The parameters chosen were Mg/(Mg+Fe),
473 Mg/(Mg+$^{[6]}$Fe), Mg, Mn, $^{[6]}$Fe, $^{[6]}$Al, Ti, (Mg+Mn+$^{[6]}$Fe) / (Ti+Cr+$^{[6]}$Al), Si, $^{[4]}$Al/Si, K, $^{[A]}$[ ], Na,
474 (K+$^{[A]}$[ ])/Na, K/($^{[A]}$[ ]+Na), Ca, Ca/$^{[8]}$Fe, *T* (K), and ln *P* (bar). The rationale for this choice of
475 parameters was 1) to test specific parameters suggested by Sato et al. (2005), *i.e.* Mg#, $^{[4]}$Al = 8-
476 Si, and *T*, 2) to test additional parameters related to the octahedral site occupancy of Mg and Fe,
477 given the local chemical properties of Fe-Cl affinity and Mg-Cl antipathy (Oberti et al., 1993b;
478 Zhang et al., 2012), 3) to test other parameters related to the size of the amphibole lattice, which
479 should correlate positively with the ability of the lattice to house the large Cl anion (Enami et al.,
480 1992; Morrison, 1991; Oberti et al., 1993b; Zhang et al., 2012), and 4) to avoid parameters
481 directly related to the oxidation state of iron or the water content of the system, so that the
482 resulting regression equations could be used in the combined model described in the next
483 section. It is noteworthy, regarding the last point, that one does observe good correlation

484 between ln K_{Cl} and regressed equations that include parameters depending on the Fe redox state
485 of the amphibole (Fe^{2+}, Fe^{3+}, $Mg\#_{ferrous}$ ($Mg/(Mg+Fe^{2+})$, $^{[6]}Mg\#_{ferrous}$ ($Mg/(Mg+^{[6]}Fe^{2+})$) and the
486 $f(H_2O)$ of the system.
487
488 Our regression model equation coefficients and standard errors are given in Table 1,
489 while the entire regression report is given for each model in Supplemental Tables 4.1-4.4. For
490 comparison, we also include the results of our methodology applied to the analytical data of Sato
491 et al. (2005) alone (Table 1 and Supplemental Table 4.5). From a statistical standpoint, the
492 resulting equations are acceptable descriptions of the global dataset. Our R-values range from
493 0.86 to 0.95 (*cf.* the 0.82 reported by Sato et al. 2005), R^2 from 0.70 to 0.84, and the F-statistics
494 (33 to 38) indicate very high confidence in the significance of modeled parameters to the
495 variation in ln K_{Cl}. The Sato-alone model presents a close correlation between observed and
496 predicted K_{Cl} values ($R = 0.97$, $R^2 = 0.95$, $F = 95$). We note that Sato et al. (2005) cite as a
497 possible source of error "the assumption of the stoichiometric anionic contents of hornblende"
498 (i.e. the assumption that 2 = OH + F + Cl), and our results suggest that not only is this in fact a
499 source of error, but that calculating the oxo-component and amphibole OH using the reversed
500 Popp et al. (2006) methodology presented in the previous section provides a significant
501 improvement in our ability to model Cl partitioning in amphibole.
502 Several points seem worthy of note from the standpoint of crystal chemistry:
503 • Mg/Fe-related parameters appear in all models, as expected. We regressed models with
504 total Fe, but eventually discarded this term from the list used to generate the final models
505 since total Fe = $^{[6]}Fe + (2 - Ca)$. The total Mg# was left in, but was eventually removed
506 from all models save the Sato-only model in favor of $^{[6]}Mg\#$, which makes sense since

the O(3) site is distant from the 8-fold site where some of the Fe resides; however, there is a small difference in the degree to which changing this parameter affects its overall correlation with ln K_{Cl} (Figure 4). In the final Lesne model, ln K_{Cl} is positively correlated with $^{[6]}$Fe and negatively correlated with Mg, as expected. The final Dixon model retains only Mg.

- Other octahedral site parameters are not well correlated with ln K_{Cl}. The ratio (Mg+Mn+$^{[6]}$Fe) / (Ti+Cr+$^{[6]}$Al) remains in the 8 parameter Lesne model, but the sign of its coefficient flips as parameters are eliminated, and it was removed from the final model. It appears that the presence of high-valence cations on the octahedral sites does not strongly affect the ability of Cl to displace OH on the O(3) site.
- Increased K (potassium) should be positively correlated with ln K_{Cl} since it is the largest common occupant of the amphibole A site and should produce an increase in the overall size of the amphibole lattice, which makes more room for the large Cl anion (Morrison, 1991; Oberti et al., 1993b). The correlation we observe is very strong (Figure 4), and K-related parameters survive into both the Dixon and Lesne final models. Sato et al. (2005) were not able to see this correlation due to the limited range of K content in their amphiboles; when we confine our dataset to only their data, K and associated ratios do not appear in our final model either. The parameter $^{[A]}$[ ] appears in the final Dixon model with a positive coefficient, and other intermediate regression results also suggest that vacant A sites increase the partitioning of Cl into amphibole relative to Na-occupied A sites. The ratio (K+$^{[A]}$[ ])/Na is positively correlated with ln K_{Cl}, but not nearly as strongly as K/(Na+$^{[A]}$[ ]).
- Sato et al. (2005) looked for a correlation between ln K_{Cl} and $^{[4]}$Al (Morrison, 1991;

Oberti et al., 1993b) and did not find one. We found some correlation with $^{[4]}$Al in preliminary models that allowed a constant term, but not in the final models, which are overall better fits to the data.

- An unexpected result is the appearance of Ca in many models, including the last Sato-only model, with a negative coefficient. We expected a positive correlation between ln K_{Cl} and Ca and/or Ca/$^{[8]}$Fe, since increasing these parameters should increase the lattice dimensions of amphibole.
- *T* refines out of our global models, although it should be kept in mind that *T* affects virtually all of the crystal chemical parameters as well. We note that, despite the very limited range of *T* considered by Sato et al. (2005), we see it included in our final model for their dataset alone with a negative coefficient, just as they found in their own analysis, as well as in many intermediate models for the whole dataset. The parameter ln *P* was retained in early Dixon models only with a negative coefficient.

We apply the eight-parameter and three-parameter models to natural igneous amphiboles and the Browne (2005) syntheses in Supplemental Table 5. We include a variety of calcic amphiboles, as well as igneous cummingtonites (Shane et al., 2007), to see what results the regressions give when extrapolated to compositions well beyond the hornblende and pargasite compositions over which they were calibrated. The K_{Cl}s calculated by the D8 and L8 models are much higher for the cummingtonites than for the calcic amphiboles and are unrealistic. Meanwhile, the D3 and L3 models give lower results for the cummingtonites than for the calcic amphiboles. As one would expect, our equations are not to be relied upon to produce reasonable results for non-calcic amphiboles. For the calcic amphiboles, the results are mostly similar and

553 fall between -2<ln K_{Cl}<0 (mostly -1.5<ln K_{Cl}<0). This signifies that Cl is incompatible in
554 amphibole relative to OH, confirming and giving some additional quantitative substance to
555 earlier conclusions from crystal chemical investigations (Morrison, 1991; Enami et al. 1992;
556 Oberti et al. 1993b; Zhang et al. 2012).

557 We also carried out the calculations of the next section given all four calculated K_{Cl}s for
558 all the calcic amphiboles. The L3 regression seems to be of the widest utility. The water
559 activities calculated with it are usually not as low as those calculated with D3 K_{Cl}s, which seem
560 unrealistic; and we consider that the 8 parameter models are underconstrained by the data. We
561 use the L3 equation in the remainder of this paper:

562 (L3) $\ln K_{Cl} = 6.59\ K / (Na +^{[A]}[\ ]) - 0.679\ Mg + 0.487\ ^{[6]}Fe$

563 Residual error in our L3 regressed values of ln K_{Cl} is shown in Figure 5, where it can be
564 seen that a great deal of the residual error is due to two outliers in the high-pressure data.
565

566 **6. Combined solution for Cl and H_2O partitioning into amphibole.** An exciting possibility is
567 provided by combining the amphibole redox model (Section 4) and our recalibrated Cl
568 partitioning model (Section 5), along with appropriate H_2O speciation and solubility models, for
569 systems where 1) ordinary suites of electron microprobe data (including Cl content) are available
570 for amphibole/glass pairs where textural evidence suggests the glass was a melt equilibrated with
571 the amphibole and 2) thermobarometric estimates, including $f(O_2)$, can be made for the system.
572 In this scenario, even without Fe speciation or H_2O content determined for either phase, these
573 values will be constrained by the models.

574 *H_2O-saturated model calculations.* If one assumes water saturation in the magma, the problem is
575 over-determined, and this can be used to check for self-consistency. The OH and $^{[O(3)]}O^{2-}$

contents of the amphibole can be calculated using the methodology of Section 4, above. Meanwhile, by assuming water saturation and choosing an appropriate speciation model, [OH] in the melt can be calculated and equation 5 can be used to determine OH and $^{[O(3)]}O^{2-}$ in the amphibole independently. If these estimates are not close, the problem may reside in the models themselves, in the assumption of water saturation, or in the representativeness of the Cl analytical data.

Supplemental Table 6 shows the results of these calculations from the same selection of amphibole/glass pairs as Supplemental Table 5, making the assumption of water saturation. Full details of the calculations are in spreadsheet form as Supplemental Table 7. For most of these systems, the calculated oxo-component is negative from the Cl partitioning model, which is equivalent to amphibole OH > 2 – F – Cl, which is of course impossible. From equation 5, there are four possibilities to explain this: 1) K_{Cl} is too small; 2) Cl determined from the amphibole is too large; 3) [Cl] determined from the glass is too small; or 4) [OH] is too large. We have selected the L3 regression to minimize the chance of possibility 1 (see previous section). We consider possibility 2 unlikely in most circumstances. Possibility 3 suggests that Cl has been lost from the glass either in its natural environment by degassing, or during sample preparation, or under the microprobe beam, all of which are important possible sources of non-representativeness. The best samples for the methodology we describe would be amphiboles within glassy melt inclusions or within the interior of large masses of glass. Glasses exposed directly to air as hot ejecta are likely to have degassed Cl, and unfortunately all the glasses in this table were so exposed. Possibility 4 suggests error in the assumption of water saturation, or potentially in the melt H_2O speciation model. In the circumstances, we believe degassing of Cl from the ejecta glass and magma undersaturation in H_2O during amphibole crystallization are the

two most important factors in explaining the negative values of $^{[O(3)]}O^{2-}$ in our model results for these volcanic amphibole/glass pairs.

H_2O-undersaturated model calculation. If the magma was not water-saturated, one can arrive at a single determination of OH and $^{[O(3)]}O^{2-}$ in the amphibole and H_2O content of the melt by combining the constraints of the amphibole redox model, the Cl partitioning model, speciation equations (Zhang and Ni, 2010), and an undersaturated water activity/fugacity model (Burnham, 1997). We manipulate the amphibole redox equation (3) as follows:

(3a) $$f(H_2) = K_x X^2(Fe^{2+}) X^2(OH) / [28.94 X^2(Fe^{3+}) X^2_{oxo}]$$

(3b) $$f(H_2O) = K_f(H_2O) f^{1/2}(O_2) K_x X^2(Fe^{2+}) X^2(OH) / [28.94 X^2(Fe^{3+}) X^2_{oxo}]$$

(3c) $$a(H_2O) = K_f(H_2O) f^{1/2}(O_2) K_x X^2(Fe^{2+}) X^2(OH) / [28.94 f^o(H_2O) X^2(Fe^{3+}) X^2_{oxo}]$$

where $K_f(H_2O)$ is the equilibrium constant for the formation of H_2O, and $f^o(H_2O)$ is the fugacity of pure H_2O vapor at the P and T being considered.

We recast the Cl partitioning coefficient equation (5) in the following form:

(5a) $$K_{Cl} \cdot ([Cl] / X_{Cl}) \cdot X_{OH} = [OH]$$

The H_2O speciation equations are (Zhang and Ni, 2010; Zhang, 1999):

$$K_2 = [OH]^2 / ([H_2O]_m[O])$$

(6) $$[H_2O]_t = [H_2O]_m + [OH]/2$$

$$[O] = 1 - [H_2O]_m - [OH]$$

622

623 The Burnham relation takes one of two forms depending on whether $\chi(H_2O) < 0.5$
624 (Burnham, 1997; Burnham and Nekvasil, 1986):

625

626 (7a) $a(H_2O) = k_w \chi^2(H_2O)$, $\chi(H_2O) < 0.5$;

627 (7b) $a(H_2O) = 0.25\, k_w\, e^{(6.52-2667/T)(\chi(H_2O)-0.5)}$, $\chi(H_2O) > 0.5$.

628

629 where k_w also has P and T dependence. Note that the Burnham mole fraction of H_2O in melt, χ
630 (H_2O), can be calculated from the Stolper/Zhang mole fraction $[H_2O]_t$ and vice-versa given the
631 anhydrous glass composition (Appendix 1).

632 Together with the amphibole stoichiometry relations (equation 4), these equations can be
633 substituted into one another to form a single equation in a single unknown: a twelfth-order
634 polynomial equation in X_{oxo} for the case of low $\chi(H_2O)$, or a complicated exponential equation if
635 the high $\chi(H_2O)$ formula is appropriate. Fortunately, the mole fraction constraint is high enough
636 that the solubility bound is often exceeded before the high H_2O version of the equation need be
637 used. These equations can be solved by numeric methods, although their sensitivity to input
638 parameters is high and care must be taken to avoid false roots and local minima when using a
639 numeric solver routine. More than one root for X_{oxo} can often be found, and although starting
640 with a low trial value for oxo-component (*e.g.*, 0.1 apfu) is usually a good way to find the root of
641 interest (which we take to be the lowest positive root), sometimes the Excel solver will overshoot
642 a root and settle into a higher one. It will also sometimes try and fail to find a lower root until
643 the trial value is raised sufficiently. A detailed mathematical treatment of these equations is
644 beyond the scope of this paper, but looking at several example forms suggests that, for the low-

water version, the appropriate root for X_{oxo} is a degenerate root, and when evaluating the function using real numbers and real software, rounding errors often cause the function to "stop" slightly above 0, as can be seen when graphing the function in a computer algebra system such as Maxima.

Returning to the calcic amphibole/glass pairs we have assembled, Supplemental Tables 8 gives full details of these calculations and Supplemental Table 9 show the results. The low-water equation has a viable solution for X_{oxo} for all samples, although the solution for the synthetic amphibole RDT-A-2 is above 0.50 $\chi(H_2O)$, and the high-H_2O equation *cannot* be solved for a meaningful root. Nearly all amphibole-glass pairs have calculated water activities well below 0.5, indicating that they probably crystallized from H_2O-undersaturated melts. However, the composite equation compensates for any postcrystallization loss of Cl from the melt (whether from degassing or sample handling) by depressing melt [OH], and therefore water activity and hydrogen fugacity as well, resulting in higher X_{oxo} and lower $a(H_2O)$. Amphibole requires a significant supply of H_2O (or, in other circumstances, F) in order to form. Thus, the very low H_2O activities in Supplemental Table 9 seem unlikely to record actual amphibole formation conditions. We can instead interpret these as evidence of Cl degassing from the associated glass. The high water activities in Supplemental Table 9, or equivalently, the good matches on Supplemental Table 6 between the two determinations of amphibole oxo-component suggest that not only was the melt/glass nearly water saturated when the amphibole crystallized, but also that these glasses have not degassed much Cl since that time. For example, both amphibole analyses from sample 92MHR9-1 from Redoubt volcano, an andesite, give calculated results that suggest that the glasses in this sample retain a Cl signature from conditions at or near the crystallization conditions for the amphibole. The other Redoubt samples are dacites that likely had been in the

668 magma chamber for some time, and whose glasses record a more degassed magma state than the
669 amphiboles (Wolf and Eichelberger, 1997).
670
671 **7. Applicability of the models.**
672 The reader will appreciate that the actual model equations presented in Table 1 are to be
673 regarded as estimates. The Popp amphibole redox equation, which we use both directly and
674 indirectly to recalibrate the Sato chlorine partitioning equation, has been calibrated over a bare
675 handful of amphibole compositions. There is an unquantifiable amount of error involved in thus
676 extrapolating Popp et al. (2006)'s expression to hornblendes and edenites, which may
677 overshadow the errors calculated in our linear regression results in Supplemental Tables 4.1 to
678 4.5. The fact that we get sensible results by using this equation suggests that Popp et al. (2006)'s
679 K_x does not vary hugely over the range of calcic amphibole compositions considered in this
680 paper, but it remains to show the actual size of this variance by conducting further experiments
681 and recalibrating the expression for K_x. Likewise, the chlorine partitioning constant K_{Cl} is in
682 need of recalibration using measured Fe^{3+}/Fe^{2+} and $OH/^{[O(3)]}O^{2-}$ values, rather than resorting to
683 modeling to estimate them; and it would be of great interest to calibrate a fluorine analog to the
684 Sato equation at the same time (Zhang et al., 2012).
685 We hope that this paper shows the value of conducting such work. With adequate
686 characterization of amphibole (Hawthorne and Oberti, 2007a), an enormous amount of
687 geochemical information can be gleaned about its formation environment, whether igneous,
688 hydrothermal, metasomatic, or metamorphic; after all, four anions and the vast majority of
689 cations, from Li to Pb, can be housed easily in the structure of natural amphiboles (Adam and
690 Green, 1994, 2006; Leake et al., 1997). While H_2O is the volatile of greatest interest in

691 magmatic systems on nearly any rocky body including Mars, the Moon, and even chondrite
692 meteorite parent bodies (McCanta et al., 2008), H is impossible to analyze via the ordinary
693 workhorse of chemical analysis, the electron microprobe. The use of alternative analytical
694 techniques such as SIMS to find H contents of geological materials is uncommon, although it is
695 expected to increase in the future (Hawthorne and Oberti, 2007a). Likewise, Fe is the main
696 redox-active metal in igneous systems, but its oxidation state is regularly left undetermined.
697 Mossbauer spectroscopy is the chief alternative for exploring the oxidation state of Fe (Gunter et
698 al., 2003), but Mossbauer spectrometers may never be widely disseminated analytical
699 instruments. Synchrotron techniques can be used to determine the Fe redox of mineral samples,
700 and are essential for studying certain kinds of difficult (e.g., small) samples (Gunter et al., 2011),
701 but synchrotron analyses involve applications for beamtime and significant investment of time
702 by facility personnel. The potential to evaluate Fe redox state with electron microprobe data
703 continues to be explored (Enders et al., 2000; Lamb et al., 2012), but such analyses have yet to
704 become reliable and routine.

705 Therefore, using the Cl contents of amphibole and glass as an indirect means to
706 determine the oxidation state of Fe in amphibole and the H_2O content of both amphibole and
707 melt is a potentially valuable way of extending the reach of conventional analytical techniques.
708 As we have seen, the results we get from pyroclastic glass may not be representative due to Cl
709 degassing, but low water activities calculated from such glass/amphibole pairs can signal relative
710 amounts of Cl degassing, as for the Redoubt rocks discussed above. This is in itself interesting
711 information.

712 Chambefort et al. (2013) explore the volatile budgets of a magmatic system using an
713 extensive collection of amphibole analyses. We applaud this work and consider it a good

example of a study that uses amphibole chemistry to provide important clues with which to interpret magma chamber processes. However, their use of amphibole properties to constrain magma volatile behaviors is hampered due to their use of Fe redox conditions calculated from the Leake et al. (1997) methodology. Thus, they see no or very weak correlations between Fe species, H_2O contents, and H isotopic ratios; however, given the negligible correlation between reliably determined and traditional norm-calculated Fe_2O_3 contents (Hawthorne and Oberti 2007a, Figure 2) this is unsurprising. Thus their interpretation of amphibole dehydration by means of opening *vacancies* on the O(3) site (Demeny et al., 2006), rather than dehydrogenation according to equation 1, is open to dispute. Use of the Popp equation, narrowly calibrated as it may be, is an advance over calculating Fe speciation by a largely arbitrary choice of cation norm, as we have argued above. Further, consideration of glass compositions and Cl partitioning could have assisted Chambefort et al. (2013) in interpreting the Cl content of different amphibole grains and their relationship to the style of magmatism, as well as the H_2O content of the amphiboles.

Having a better constrained crystal chemical model for amphibole-melt Cl partitioning could enhance understanding of the amphibole and plagioclase thermobarometers (Blundy and Holland, 1990; Holland and Blundy, 1994), which Chambefort et al. (2013) use extensively. Humphreys et al. (2009) also use these in conjunction with the Sato model to examine the variation in Cl content of different magmas crystallizing hornblende in the Soufriere Hills volcanic system, while using A site occupancy to gauge temperature. Since the contents of the A site appear to play an important role in governing Cl partitioning, there is unacknowledged complexity in the chemical equilibrium calculations that Humphreys et al. (2009) use to interpret their data.

Acknowledgments. We gratefully acknowledge support from NASA MFR grant # NNX13AG35. We thank Hiroaki Sato, Gordon Moore, and an anonymous reviewer, as well as our associate editor Rosario Esposito, for their helpful and timely comments. We thank Filippo Ridolfi, Philipp Ruprecht, Pavel Izebekov, and Stephen Turner for generous sharing of data which appear in Supplemental Table 1. We would also like to thank Bob Popp and Wally Lamb for sharing data, clarifying a few details in their papers, and discussing many of the thermodynamic issues related to amphibole dehydrogenation. Lastly, we also thank Tony Withers for his implementation of a routine to calculate H_2O fugacities from the data and equations of Pitzer and Sterner (1994) and Sterner and Pitzer (1994).

Appendix 1: H_2O solubility, speciation, and activity models

The solubility of H_2O in silicate melts is a subject of great interest to petrologists and has received a correspondingly large amount of attention in the literature. Any model that is not completely empirical will depend on some understanding of the speciation of H_2O in the melt. Until the publication of Stolper (1982), the consensus in the literature was that H_2O completely dissociated to OH groups in the melt up to a certain large concentration of H_2O. The final version of the most successful model incorporating this hypothesis is found in Burnham (1997); Burnham and Nekvasil (1986). Although the work of Stolper and others confirmed that this theory is flawed because intact H_2O molecules are found in hydrated silicate melts of all concentrations (Ohlhorst et al., 2001), and later solubility models provide improved predictions in a variety of melts under a variety of *T, P* conditions (Papale, 1997), the Burnham model is still quantitatively adequate for many purposes (Baker and Alletti, 2012).

We employ the Burnham model in this paper because it is the only model to attempt to describe the thermodynamic properties of H_2O in melts *not* in equilibrium with a vapor phase. This is displayed graphically in Burnham and Davis (1974), Figures 8 to 12. We produce a similar figure for illustration here (Figure A.1) along with the solubility curve of Moore et al. (1998) for the Sato et al. (2005) sample 298. The curved line in the figure is the solubility relation, while the straight lines show the subsaturation fugacity-mole fraction relationship calculated from Burnham (1997) at overall pressures of 1, 2, 3...8 kbar, including the adjustment for Al content of the melt, which we have simplified as follows:

$$\ln k_w^{feldspar} = \ln k_w^{melt} + 0.47\,[1 - 4\,\mathrm{Al}/(\mathrm{Al}+\mathrm{Si})] \quad \text{(A.1)}$$

where Al and Si are molar quantities of each cation in the melt. The correction term equals 0 for any melt with the same Al/(Al+Si) content as feldspar, is negative for relatively Al-enriched melts (like nepheline melt) and is positive for relatively Al-depleted melts.

For solubility relationships, we employ the model of Moore et al. (1998). There are more complex, accurate, and up-to-date models in the literature (Dixon, 1997; Iacono-Marziano et al., 2012; Newman and Lowenstern, 2002; Papale et al., 2006; Witham et al., 2012), but the model of Moore et al. (1998) is flexible, with compositional terms refined over a creditable variety of melt chemistries, and is much simpler to implement than the other models. For the purposes of this paper, which is meant as an illustration of methodology as much as it is meant to provide quantitative modeling information, the Moore et al. (1998) model serves well.

It seems appropriate to remind the reader here that there are at least three different methods of calculating the mole fraction of H_2O and other components in melts: the Burnham 8O basis (Burnham, 1997), the Stolper/Zhang 1O basis (Stolper, 1982; Zhang, 1999), and the more intuitive sum-of-oxides basis employed by Moore et al. (1998). The variety of bases reflects the differences in theoretical underpinnings, or lack thereof, of the various models, as well as the fundamental ambiguity in defining a molar quantity of melt. Since Moore et al. (1998) do not describe their methodology, and it differs greatly from the others but is nevertheless simple to explain (Moore, personal communication, 2013), we do so here for the benefit of the reader. Their mole fractions are calculated by adding up the number of moles of each oxide component (SiO_2, Al_2O_3, etc.) to serve as the denominator of the mole fraction. Thus $\chi(H_2O) = n(H_2O)/(n(SiO_2) + n(Al_2O_3) + ... + n(H_2O))$. This will generally result in a number not quite twice the size of a 1O mole fraction.

Appendix 2: Statistical Procedure

We calculated a multiple linear regression model for the entire family of parameters for each separate determination of ln K_{Cl} (*i.e.*, both the Lesne and Dixon determinations). The basic methodology was that the parameter with the highest *p* value was rejected, and the model recalculated with the remaining parameters, the process being repeated until all parameters had *p* values below 0.09-0.10. We tried this on many, many collections of parameters; the following discussion is greatly condensed. Based on the results of several dozen regressions, we found that eliminating the constant term systematically gave better results, and so the final models have no constant term. Since Excel will only calculate regressions on up to 16 variables, we collected the element parameters and the ratio parameters separately, regressed each collection along with *T* and ln *P*, rejected a total of 3 parameters, then gathered the remainder back into a single set and proceeded as above. This process resulted in two models with 8 variable terms (Dixon 8 or D8 and Lesne 8 or L8), the other 11 parameters being rejected. These models had mixtures of ratios and element contents and therefore had some coefficients with counterintuitive signs. In addition, since the dataset has only 39 entries, the data:parameter ratio was only ~5:1. For both these reasons, we continued rejecting parameters employing 1) *p* values, 2) the desire to eliminate either ratio parameters or their constituent element parameters rather than leaving both a ratio and its constituents in the final models, and 3) our best judgment based on the literature of amphibole crystal chemistry. In the end, the final model equations had 3 terms (Dixon 3 or D3 and Lesne 3 or L3).

References

Adam, J. and Green, T.H. (1994) The effects of pressure and temperature on the partitioning of Ti, Sr and REE between amphibole, clinopyroxene and basanitic melts. Chemical Geology, 117, 219-233.

Adam, J. and Green, T. (2006) Trace element partitioning between mica- and amphibole-bearing garnet lherzolite and hydrous basanitic melt: 1. Experimental results and the investigation of controls on partitioning behaviour. Contributions to Mineralogy and Petrology, 152, 1-17.

Adam, J., Oberti, R., Camara, F., and Green, T.H. (2007) An electron microprobe, LAM-ICP-MS and single-crystal X-ray structure refinement study of the effects of pressure, melt-H_2O concentration and $f(O_2)$ on experimentally produced basaltic amphiboles. European Journal of Mineralogy, 19, 641-655.

Baker, D.R. and Alletti, M. (2012) Fluid saturation and volatile partitioning between melts and hydrous fluids in crustal magmatic systems: The contribution of experimental measurements and solubility models. Earth-Science Reviews, 114, 298-324.

Blundy, J.D. and Holland, T.J.B. (1990) Calcic amphibole equilibria and a new amphibole-plagioclase geothermometer. Contributions to Mineralogy and Petrology, 104, 208-224.

Boyce, J.W., Liu, Y., Rossman, G.R., Guan, Y., Eiler, J.M., Stolper, E.M., and Taylor, L.A. (2010) Lunar apatite with terrestrial volatile abundances. Nature, 466, 466-469.

Browne, B.L. (2005) Petrologic and experimental constraints on magma mingling and ascent: examples from Japan and Alaska. Geology and Geophysics, Ph.D. University of Alaska, Fairbanks.

Burnham, C.W. (1997) Magmas and hydrothermal fluids. In H.L. Barnes, Ed. Geochemistry of

hydrothermal ore deposits, p. 972. John Wiley & Sons, New York.

Burnham, C.W. and Davis, F.A. (1974) The role of H_2O in silicate melts II: Thermodynamic and phase relations in the system $NaAlSi_3O_8$-H_2O to 10 kilobars, 700 ^{o} to 1000 ^{o}C. American Journal of Science, 274, 902-940.

Burnham, C.W. and Nekvasil, H. (1986) Equilibrium properties of granite pegmatite magmas. American Mineralogist, 71, 239-263.

Chambefort, I., Dilles, J.H., and Longo, A.A. (2013) Amphibole geochemistry of the Yanacocha Volcanics, Peru: Evidence for diverse sources of magmatic volatiles related to gold ores. Journal of Petrology, 54, 1017-1048.

Chambers, J.A. and Kohn, M.J. (2012) Titanium in muscovite, biotite, and hornblende: Modeling, thermometry, and rutile activities of metapelites and amphibolites. American Mineralogist, 97, 543-555.

Deer, W.A., Howie, R.A., and Zussman, J. (1997) Double-chain silicates. 764 p. Geological Society, London.

Demeny, A., Vennemann, T.W., Harangi, S., Homonnay, Z., and Forizs, I. (2006) H_2O-δD-Fe(III) relations of dehydrogenation and dehydration processes in magmatic amphiboles. Rapid Communications in Mass Spectrometry, 20, 919-925.

Dixon, J.E. (1997) Degassing of alkalic basalts. American Mineralogist, 82, 368-378.

Dixon, J.E., Stolper, E.M., and Holloway, J.R. (1995) An experimental study of water and carbon dioxide solubilities in mid ocean ridge basaltic liquids. 1. Calibration and solubility models. Journal of Petrology, 36, 1607-1631.

Dyar, M.D., McGuire, A.V., and Mackwell, S.J. (1992) Fe^{3+}/H^{+} and D/H in kaersutites: Misleading indicators of mantle source fugacities. Geology, 20, 565-568.

Dyar, M.D., Mackwell, S.J., McGurnn, A.N.V., Cnoss, L.R., and RonenrsoN, J.D. (1993) Crystal chemistry of Fe^{3+} and H^{+} in mantle kaersutite: Implications for mantle metasomatism. American Mineralogist, 78, 968-979.

Enami, M., Liou, J.G., and Bird, D.K. (1992) Cl-bearing amphibole in the Salton Sea geothermal system, California. Canadian Mineralogist, 30, 1077-1092.

Enders, M., Speer, D., Maresch, W.V., and McCammon, C.A. (2000) Ferric/ferrous iron ratios in sodic amphiboles: Mossbauer analysis, stoichiometry-based model calculations and the high-resolution microanalytical flank method. Contributions to Mineralogy and Petrology, 140, 135-147.

Filiberto, J. and Treiman, A.H. (2009a) Martian magmas contained abundant chlorine, but little water. Geology, 37, 1087-1090.

Filiberto, J. and Treiman, A. (2009b) The effect of chlorine on the liquidus of basalt: First results and implications for basalt genesis on Mars and Earth. Chemical Geology, 263, 60-68.

Garcia, M.O., Muenow, D.W., and Liu, N.W.K. (1980) Volatiles in Ti-rich amphibole megacrysts, southwest USA. American Mineralogist, 65, 306-312.

Gunter, M.E., Dyar, M.D., Twamley, B., Foit, F.F., and Cornelius, S. (2003) Composition, $Fe^{3+}/\sum Fe$, and crystal structure of non-asbestiform and asbestiform amphiboles from Libby, Montana, USA. American Mineralogist, 88, 1970-1978.

Gunter, M.E., Dyar, M.D., Lanzirotti, A., Tucker, J.M., and Speicher, E.A. (2011) Differences in Fe-redox for asbestiform and nonasbestiform amphiboles from the former vermiculite mine, near Libby, Montana, USA. American Mineralogist, 96, 1414-1417.

Hauri, E.H., Gaetani, G.A., and Green, T.H. (2006) Partitioning of water during melting of the Earth's upper mantle at H_2O-undersaturated conditions. Earth and Planetary Science

884 Letters, 248, 715-734.
885 Hawthorne, F.C. and Oberti, R. (2007a) Amphiboles: Crystal chemistry. Reviews in Mineralogy
886 and Geochemistry, 67, 1-54.
887 -. (2007b) Classification of the amphiboles. Reviews in Mineralogy and Geochemistry, 67, 55-
888 88.
889 Hawthorne, F.C., Oberti, R., and Sardone, N. (1996a) Sodium at the a site in clinoamphiboles:
890 The effects of composition on patterns of order. Canadian Mineralogist, 34, 577-593.
891 Hawthorne, F.C., Oberti, R., Ungaretti, L., and Grice, J.D. (1996b) A new hyper-calcic
892 amphibole with Ca at the A site: Fluor-cannilloite from Pargas, Finland. American
893 Mineralogist, 81, 995-1002.
894 Hawthorne, F.C., Oberti, R., Harlow, G.E., Maresch, W.V., Martin, R.F., Schumacher, J.C., and
895 Welch, M.D. (2012) Nomenclature of the amphibole supergroup. American Mineralogist,
896 97, 2031-2048.
897 Holland, T. and Blundy, J. (1994) Nonideal interactions in calcic amphiboles and their bearing on
898 amphibole-plagioclase thermometry. Contributions to Mineralogy and Petrology, 116,
899 433-447.
900 Holloway, J.R. and Ford, C.E. (1975) Fluid-absent melting of fluoro-hydroxy amphibole
901 pargasite to 35 kilobars. Earth and Planetary Science Letters, 25, 44-48.
902 Holloway, J.R., Pan, V., and Gudmundsson, G. (1992) High-pressure fluid-absent melting
903 experiments in the presence of graphite: Oxygen fugacity, ferric-ferrous ratio and
904 dissolved CO_2. European Journal of Mineralogy, 4, 105-114.
905 Humphreys, M.C.S., Edmonds, M., Christopher, T., and Hards, V. (2009) Chlorine variations in
906 the magma of Soufrière Hills Volcano, Montserrat: Insights from Cl in hornblende and

melt inclusions. Geochimica et Cosmochimica Acta, 73, 5693-5708.

Iacono-Marziano, G., Morizet, Y., Le Trong, E., and Gaillard, F. (2012) New experimental data and semi-empirical parameterization of H_2O-CO_2 solubility in mafic melts. Geochimica Et Cosmochimica Acta, 97, 1-23.

Iman, R.L. (1994) Chapter 13: Multiple Linear Regression. A Data-Based Approach To Statistics. Duxbury Press, Belmont, CA.

Jenkins, D.M. (2011) The transition from blueschist to greenschist facies modeled by the reaction glaucophane+2 diopside+2 quartz = tremolite+2 albite. Contributions to Mineralogy and Petrology, 162, 725-738.

Johnson, N.M. and Fegley, B. (2003) Tremolite decomposition on Venus II. Products, kinetics, and mechanism. Icarus, 164, 317-333.

King, P.L., Hervig, R.L., Holloway, J.R., Vennemann, T.W., and Righter, K. (1999) Oxy-substitution and dehydrogenation in mantle-derived amphibole megacrysts. Geochimica et Cosmochimica Acta, 63, 3635-3651.

King, P.L., Hervig, R.L., Holloway, J.R., Delaney, J.S., and Dyar, M.D. (2000) Partitioning of Fe^{3+}/Fe_{total} between amphibole and basanitic melt as a function of oxygen fugacity. Earth and Planetary Science Letters, 178, 97-112.

Lamb, W.M. and Popp, R.K. (2009) Amphibole equilibria in mantle rocks: Determining values of mantle $a(H_2O)$ and implications for mantle H2O contents. American Mineralogist, 94, 41-52.

Lamb, W.M., Guillemette, R., Popp, R.K., Fritz, S.J., and Chmiel, G.J. (2012) Determination of Fe^{3+}/Fe using the electron microprobe: A calibration for amphiboles. American Mineralogist, 97, 951-961.

930 Leake, B.E. (1968) A catalog of analyzed calciferous and subcalciferous amphiboles together
931 with their nomenclature and associated minerals. Special papers (Geological Society of
932 America), 210 p., Washington, D.C.
933 Leake, B.E., Woolley, A.R., Arps, C.E.S., Birch, W.D., Gilbert, M.C., Grice, J.D., Hawthorne,
934 F.C., Kato, A., Kisch, H.J., Krivovichev, V.G., Linthout, K., Laird, J., Mandarino, J.A.,
935 Maresch, W.V., Nickel, E.H., Rock, N.M.S., Schumacher, J.C., Smith, D.C., Stephenson,
936 N.C.N., Ungaretti, L., Whittaker, E.J.W., and Guo, Y.Z. (1997) Nomenclature of
937 amphiboles: Report of the subcommittee on amphiboles of the International
938 Mineralogical Association, Commission on New Minerals and Mineral Names. American
939 Mineralogist, 82, 1019-1037.
940 Lesne, P., Scaillet, B., Pichavant, M., Iacono-Marziano, G., and Beny, J.-M. (2011) The H_2O
941 solubility of alkali basaltic melts: an experimental study. Contributions to Mineralogy and
942 Petrology, 162, 133-151.
943 Liu, Y., Behrens, H., and Zhang, Y.X. (2004) The speciation of dissolved H2O in dacitic melt.
944 American Mineralogist, 89, 277-284.
945 Luhr, J.F. (2002) Petrology and geochemistry of the 1991 and 1998-1999 lava flows from Volcan
946 de Colima, Mexico: implications for the end of the current eruptive cycle. Journal of
947 Volcanology and Geothermal Research, 117, 169-194.
948 Martin, R.F. (2007) Amphiboles in the Igneous Environment. Reviews in Mineralogy and
949 Geochemistry, 67, pp. 323-358. Mineralogical Society of America, Washington, DC.
950 Mazdab, F.K. (2003) The diversity and occurrence of potassium-dominant amphiboles. Canadian
951 Mineralogist, 41, 1329-1344.
952 McCanta, M.C., Treiman, A.H., Dyar, M.D., Alexander, C.M.O.D., Rumble, D., III, and Essene,

E.J. (2008) The LaPaz Icefield 04840 meteorite: Mineralogy, metamorphism, and origin of an amphibole- and biotite-bearing R chondrite. Geochimica et Cosmochimica Acta, 72, 5757-5780.

McCubbin, F.M., Nekvasil, H., Harrington, A.D., Elardo, S.M., and Lindsley, D.H. (2008) Compositional diversity and stratification of the Martian crust: Inferences from crystallization experiments on the picrobasalt Humphrey from Gusev Crater, Mars. Journal of Geophysical Research-Planets, 113(E11).

Médard, E., McCammon, C.A., Barr, J.A., and Grove, T.L. (2008) Oxygen fugacity, temperature reproducibility, and H_2O contents of nominally anhydrous piston-cylinder experiments using graphite capsules. American Mineralogist, 93, 1838-1844.

Miller, T.P., Chertkoff, D.G., Eichelberger, J.C., and Coombs, M.L. (1999) Mount Dutton volcano, Alaska: Aleutian arc analog to Unzen volcano, Japan. Journal of Volcanology and Geothermal Research, 89, 275-301.

Minitti, M.E., Rutherford, M.J., Taylor, B.E., Dyar, M.D., and Schultz, P.H. (2008a) Assessment of shock effects on amphibole water contents and hydrogen isotope compositions: 1. Amphibolite experiments. Earth and Planetary Science Letters, 266, 46-60.

Minitti, M.E., Leshin, L.A., Dyar, M.D., Ahrens, T.J., Guan, Y., and Luo, S.-N. (2008b) Assessment of shock effects on amphibole water contents and hydrogen isotope compositions: 2. Kaersutitic amphibole experiments. Earth and Planetary Science Letters, 266, 288-302.

Moore, G., Vennemann, T., and Carmichael, I.S.E. (1998) An empirical model for the solubility of H_2O in magmas to 3 kilobars. American Mineralogist, 83, 36-42.

Morrison, J. (1991) Compositional constraints on the incorporation of Cl into amphiboles.

American Mineralogist, 76, 1920-1930.

Newman, S. and Lowenstern, J.B. (2002) VOLATILECALC: a silicate melt-H_2O-CO_2 solution model written in Visual Basic for excel. Computers & Geosciences, 28, 597-604.

Nowak, M. and Behrens, H. (2001) Water in rhyolitic magmas: getting a grip on a slippery problem. Earth and Planetary Science Letters, 184, 515-522.

Oberti, R., Hawthorne, F.C., Ungaretti, L., and Cannillo, E. (1993a) The behavior of Mn in amphiboles - Mn in richterite. European Journal of Mineralogy, 5, 43-51.

Oberti, R., Ungaretti, L., Cannillo, E., and Hawthorne, F.C. (1993b) The mechanism of Cl incorporation in amphibole. American Mineralogist, 78, 746-752.

Ohlhorst, S., Behrens, H., and Holtz, F. (2001) Compositional dependence of molar absorptivities of near-infrared OH- and H_2O bands in rhyolitic to basaltic glasses. Chemical Geology, 174, 5-20.

Papale, P. (1997) Modeling of the solubility of a one-component H_2O or CO_2 fluid in silicate liquids. Contributions to Mineralogy and Petrology, 126, 237-251.

Papale, P., Moretti, R., and Barbato, D. (2006) The compositional dependence of the saturation surface of H_2O+CO_2 fluids in silicate melts. Chemical Geology, 229, 78-95.

Patiño Douce, A.E., Roden, M.F., Chaumba, J., Fleisher, C., and Yogodzinski, G. (2011) Compositional variability of terrestrial mantle apatites, thermodynamic modeling of apatite volatile contents, and the halogen and water budgets of planetary mantles. Chemical Geology, 288, 14-31.

Pilet, S., Ulmer, P., and Villiger, S. (2010) Liquid line of descent of a basanitic liquid at 1.5 Gpa: constraints on the formation of metasomatic veins. Contributions to Mineralogy and Petrology, 159, 621-643.

999 Pitzer, K.S. and Sterner, S.M. (1994) Equations of state valid continuously from zero to extreme
1000 pressures for H_2O and CO_2. Journal of Chemical Physics, 101, 3111-3116.
1001 Popp, R.K., and Bryndzia, L.T. (1992) Statistical analyses of Fe^{3+}, Ti, and OH in kaersutite from
1002 alkalic igneous rocks and mafic mantle xenoliths. American Mineralogist 77, 1250-1257.
1003 Popp, R.K., Virgo, D., Yoder, H.S.Y.J., Hoering, T.C., and Phillips, M.W. (1995) An experimental
1004 study of phase equilbria and Fe oxy-component in kaersutitic amphibole: Implications for
1005 the $f(H_2)$ and $a(H_2O)$ in the upper mantle. American Mineralogist, 80, 534-548.
1006 Popp, R.K., Hibbert, H.A., and Lamb, W.M. (2006) Oxy-amphibole equilibria in Ti-bearing
1007 calcic amphiboles: Experimental investigation and petrologic implications for mantle-
1008 derived amphiboles. American Mineralogist, 91, 54-66.
1009 Rasmussen, K.L. and Mortensen, J.K. (2013) Magmatic petrogenesis and the evolution of
1010 (F:Cl:OH) fluid composition in barren and tungsten skarn-associated plutons using
1011 apatite and biotite compositions: Case studies from the northern Canadian Cordillera. Ore
1012 Geology Reviews, 50, 118-142.
1013 Ridolfi, F., Puerini, M., Renzulli, A., Menna, M., and Toulkeridis, T. (2008) The magmatic
1014 feeding system of El Reventador volcano (Sub-Andean zone, Ecuador) constrained by
1015 texture, mineralogy and thermobarometry of the 2002 erupted products. Journal of
1016 Volcanology and Geothermal Research, 176, 94-106.
1017 Ridolfi, F., Renzulli, A., and Puerini, M. (2010) Stability and chemical equilibrium of amphibole
1018 in calc-alkaline magmas: an overview, new thermobarometric formulations and
1019 application to subduction-related volcanoes. Contributions to Mineralogy and Petrology,
1020 160, 45-66.
1021 Sato, H., Holtz, F., Behrens, H., Botcharnikov, R., and Nakada, S. (2005) Experimental petrology

of the 1991-1995 Unzen dacite, Japan. Part II: Cl/OH partitioning between hornblende and melt and its implications for the origin of oscillatory zoning of hornblende phenocrysts. Journal of Petrology, 46, 339-354.

Saxena, S.K. and Ekstrom, T.K. (1970) Statistical chemistry of calcic amphiboles. Contributions to Mineralogy and Petrology, 26, 276.

Schumacher, J.C. (2007) Metamorphic amphiboles: Composition and coexistence. Reviews in Mineralogy and Geochemistry, 67, 359-416.

Shane, P., Martin, S.B., Smith, V.C., Beggs, K.F., Darragh, M.B., Cole, J.W., and Nairn, I.A. (2007) Multiple rhyolite magmas and basalt injection in the 17.7 ka Rerewhakaaitu eruption episode from Tarawera volcanic complex, New Zealand. Journal of Volcanology and Geothermal Research, 164, 1-26.

Silver, L. and Stolper, E. (1989) Water in albitic glasses. Journal of Petrology, 30, 667-709.

Smelik, E.A. and Veblen, D.R. (1992a) Exsolution of ca-amphibole from glaucophane and the miscibility gap between sodic and calcic amphiboles. Contributions to Mineralogy and Petrology, 112, 178-195.

-. (1992b) Exsolution of hornblende and the solubility limits of calcium in orthoamphibole. Science, 257, 1669-1672.

-. (1993) A transmission and analytical electron-microscope study of exsolution microstructures and mechanisms in the orthoamphiboles anthophyllite and gedrite. American Mineralogist, 78, 511-532.

-. (1994) Complex exsolution in glaucophane from Tillotson Peak, north-central Vermont. Canadian Mineralogist, 32, 233-255.

Smith, M.P. (2007) Metasomatic silicate chemistry at the Bayan Obo Fe-REE-Nb deposit, Inner

Mongolia, China: Contrasting chemistry and evolution of fenitising and mineralising fluids. Lithos, 93, 126-148.

Sterner, S.M. and Pitzer, K.S. (1994) An equation of state for carbon dioxide valid from zero to extreme pressures. Contributions to Mineralogy and Petrology, 117, 362-374.

Stolper, E. (1982) The speciation of water in silicate melts. Geochimica et Cosmochimica Acta, 46, 2609-2620.

Turner, S.J., Izbekov, P., and Langmuir, C. (2013) The magma plumbing system of Bezymianny Volcano: Insights from a 54 year time series of trace element whole-rock geochemistry and amphibole compositions. Journal of Volcanology and Geothermal Research, http://dx.doi.org/10.1016/j.jvolgeores.2012.12.014.

Ulmer, P. and Luth, R.W. (1991) The graphite-COH fluid equilibrium in P, T, $f(O_2)$ space - an experimental-determination to 30 kbar and 1600-degrees-C. Contributions to Mineralogy and Petrology, 106, 265-272.

Witham, F., Blundy, J., Kohn, S.C., Lesne, P., Dixon, J., Churakov, S.V., and Botcharnikov, R. (2012) SolEx: A model for mixed COHSCl-volatile solubilities and exsolved gas compositions in basalt. Computers & Geosciences, 45, 87-97.

Wolf, K.J. and Eichelberger, J.C. (1997) Syneruptive mixing, degassing, and crystallization at Redoubt Volcano, eruption of December, 1989 to May 1990. Journal of Volcanology and Geothermal Research, 75, 19-37.

Zhang, C., Holtz, F., Ma, C., Wolff, P., and Li, X. (2012) Tracing the evolution and distribution of F and Cl in plutonic systems from volatile-bearing minerals: a case study from the Liujiawa pluton (Dabie orogen, China). Contributions to Mineralogy and Petrology, 164, 859-879.

1068 Zhang, Y.X. (1999) H_2O in rhyolitic glasses and melts: Measurement, speciation, solubility, and
1069 diffusion. Reviews of Geophysics, 37, 493-516.
1070 Zhang, Y. and Ni, H. (2010) Diffusion of H, C, and O Components in Silicate Melts. In
1071 Y.X.C.D.J. Zhang, Ed. Diffusion in Minerals and Melts, Reviews in Mineralogy and
1072 Geochemistry 72, pp. 171-225.
1073 Zhu, C. and Sverjensky, D.A. (1991) Partitioning of F-Cl-OH between minerals and
1074 hydrothermal fluids. Geochimica et Cosmochimica Acta, 55, 1837-1858.
1075 Zingg, A.J. (1996) Immiscibility in Ca-amphiboles. Journal of Petrology, 37, 471-496.
1076

1077 **Table 1. Coefficients for regression equations for ln K_{Cl}.**

Models	**Dixon 8**	**Dixon 3**	**Lesne 8**	**Lesne 3**	**Sato Only**
R, R^2	0.95, 0.90	0.87, 0.77	0.95, 0.89	0.86, 0.75	0.97, 0.95
Parameters	*Coefficients*	*Coefficients*	*Coefficients*	*Coefficients*	*Coefficients*
K (apfu)	-20.0±8.5	9.2±1.9	-14.6±7.2		
K/(Na+$^{[A]}$[ ])	29.7±7.3		30.9±6.3	6.6±0.9	
Na (apfu)	10.8±2.3		20.6±4.2		
$^{[A]}$[ ] (vpfu)	12.9±2.1	3.2±0.5	20.5±4.0		
Ca (apfu)	-1.7±0.7				-5.2±0.7
Mg (apfu)	-3.4±0.7	-1.0±0.1	-4.7±1.0	-0.7±0.1	-5.2±0.4
Mg/(Mg+Fe)					39.1±5.1
$^{[6]}$Mg/($^{[6]}$Mg+$^{[6]}$Fe)	9.6±3.1				
$^{[6]}$Fe (apfu)			-3.6±1.0	0.5±0.1	3.9±0.7
(Mg+Mn+$^{[6]}$Fe) / (Ti+Cr+$^{[6]}$Al)			0.2±0.1		
T (K)			$-3.4\pm1.8\cdot10^{-3}$		$-5.9\pm1.9\cdot10^{-3}$
ln P (bar)	-0.8±0.2				

1078

1079

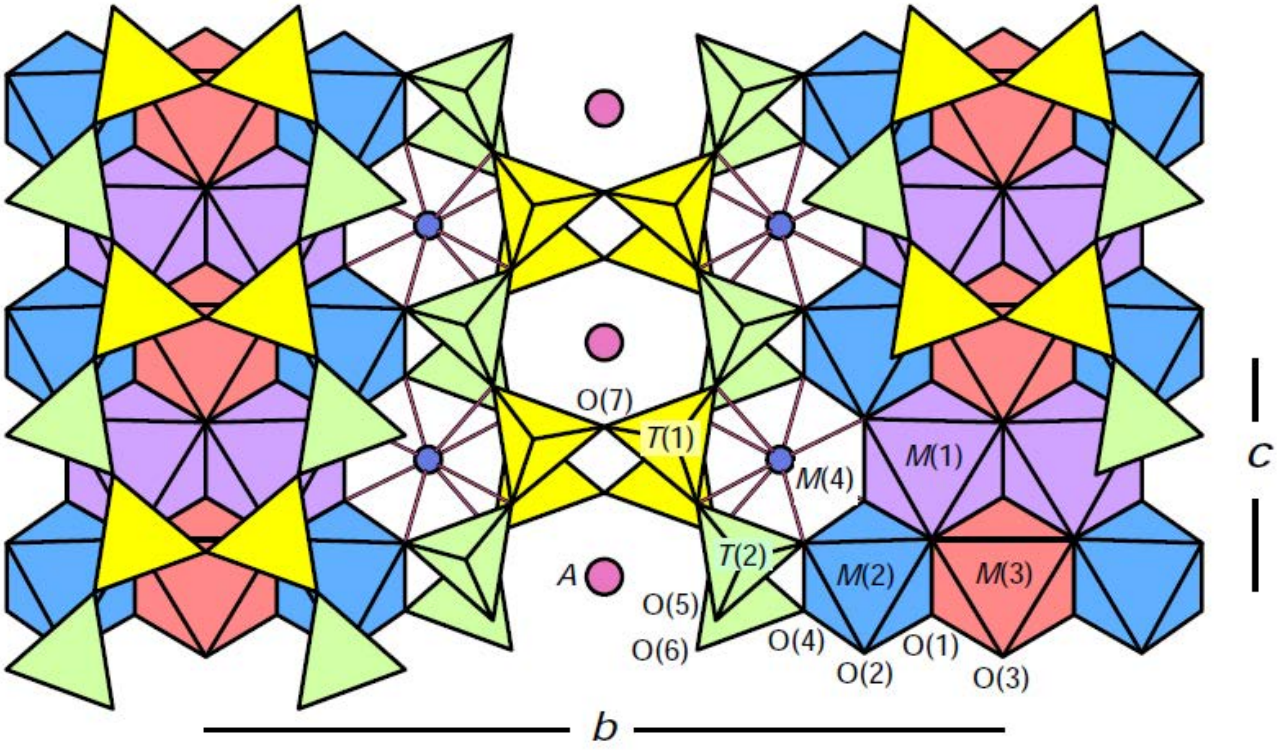

Figure 1. Structure of a typical amphibole (space group C2/*m*), from Hawthorne and Oberti (2007a). Cation sites are labeled T (4-fold sites), M (1-3: 6-fold sites; 4: 8-fold site), and A. The O(3) site contains OH, F, Cl, or O^{2-}; all other O sites contain O^{2-}.

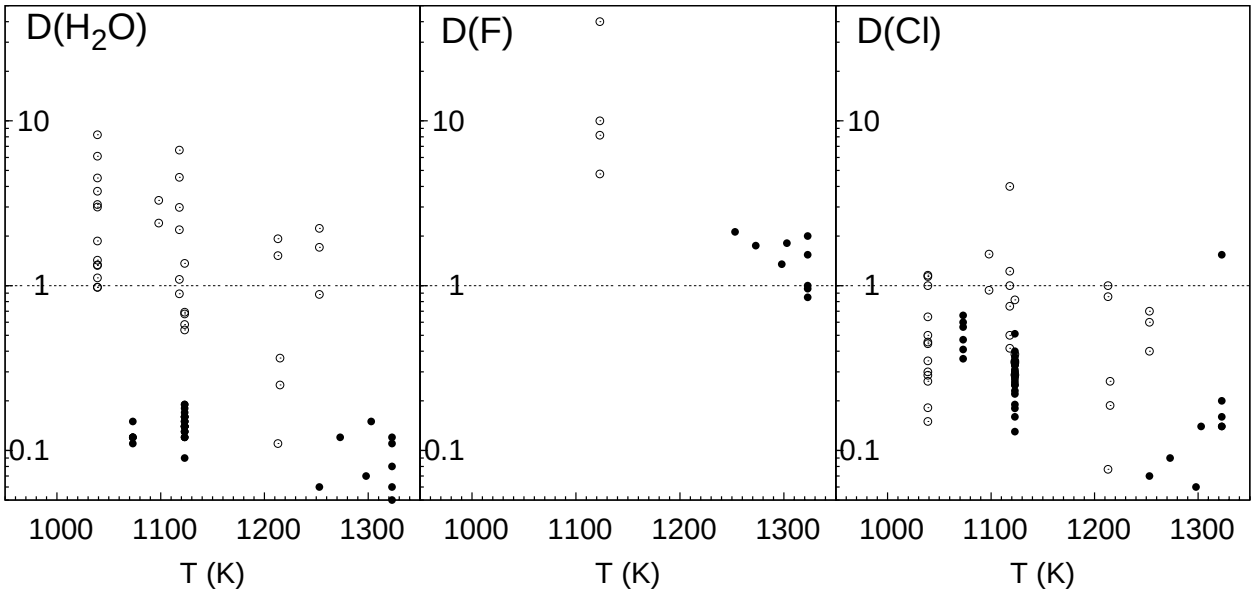

Figure 2. Bulk partition coefficients *D* for amphibole-melt (glass) pairs from synthetic (solid symbols, at or near water saturation) and natural systems (open symbols, undersaturated conditions, calculated values for H_2O from Supplemental Table 9). See Supplemental Tables 1.1, 1.2, and 1.3 (Adam and Green, 2006; Adam and Green, 1994; Adam et al., 2007; Browne, 2005; Hauri et al., 2006; Luhr, 2002; McCubbin et al., 2008; Miller et al., 1999; Ridolfi et al., 2008; Sato et al., 2005; Shane et al., 2007; Wolf and Eichelberger, 1997) for amphibole compositions.

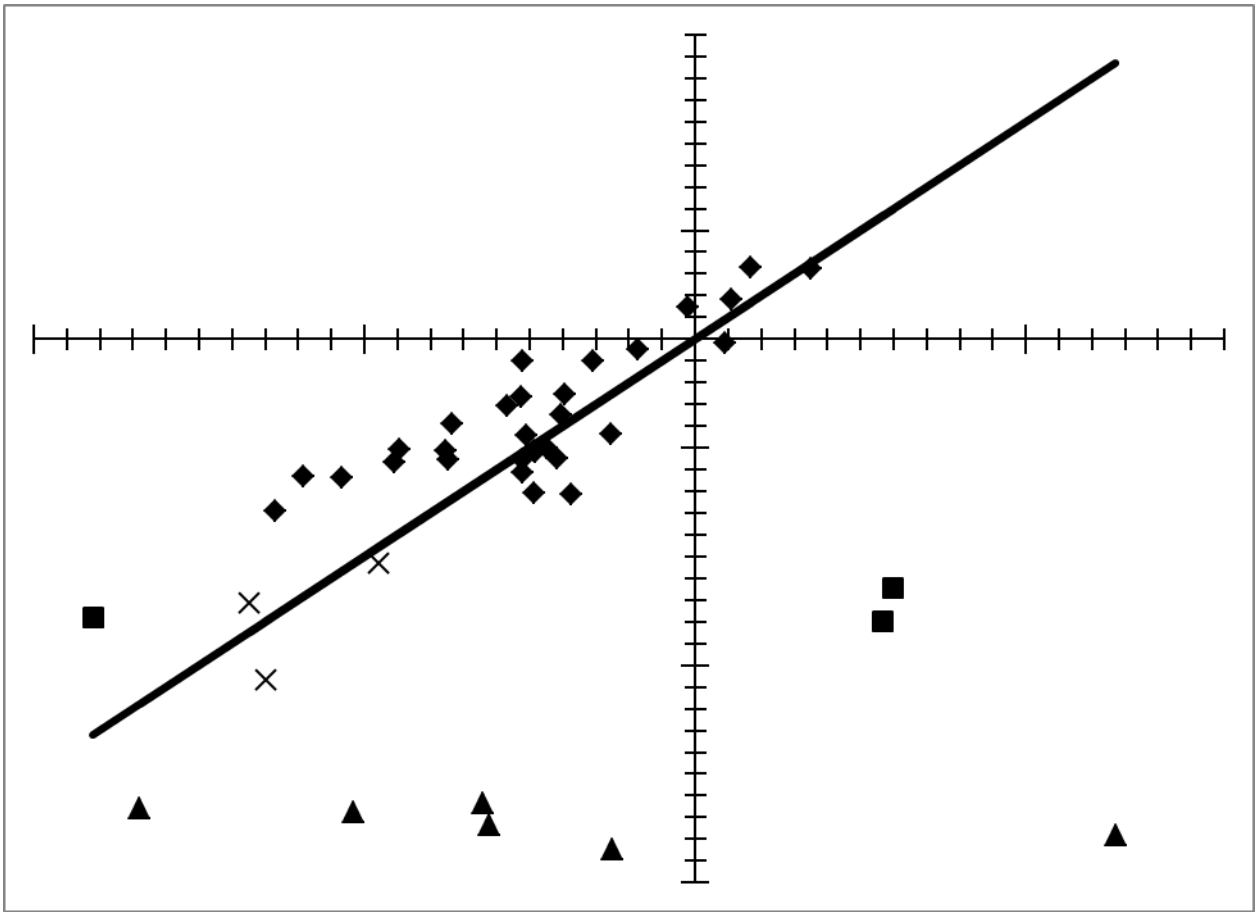

Figure 3. Plot of ln K_{Cl} experimental vs. calculated (Sato et al., 2005) from Supplemental Table 3. Diamonds: Sato et al. (2005). Triangles: high-pressure data (Adam and Green, 2006; Adam and Green, 1994; Adam et al., 2007; Hauri et al., 2006). Crosses: McCubbin et al. (2008). Squares: Browne (2005). Line is ideal fit (experimental = calculated). Axis ticks are marked every 0.1 log unit.

1102

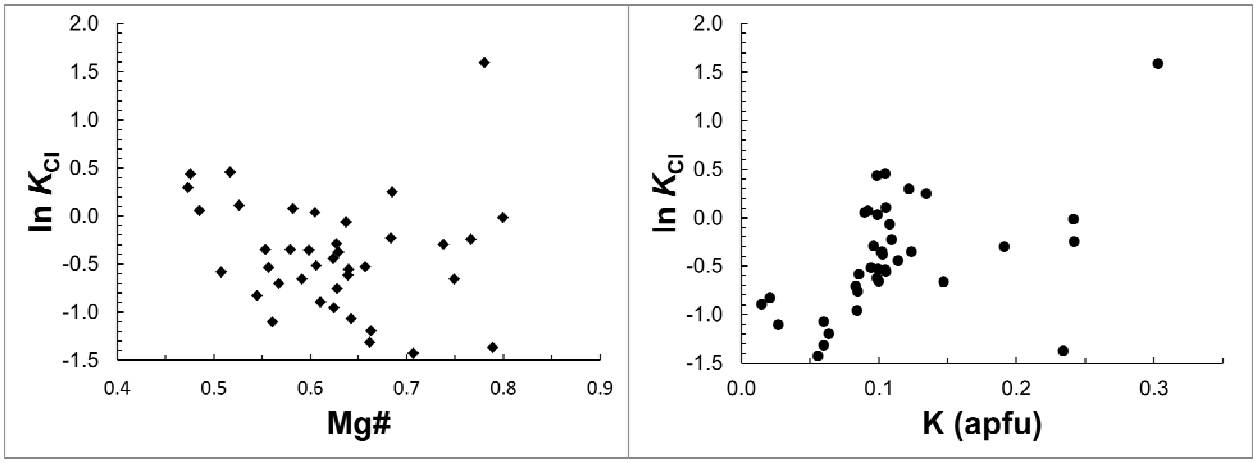

1103 **Figure 4. Left: ln K_{Cl} calculated using T-dependent melt H_2O speciation for all data (Lesne**

1104 **et al., 2011; Liu et al., 2004) versus Mg#. Right: ln K_{Cl} versus K (apfu).**

1105

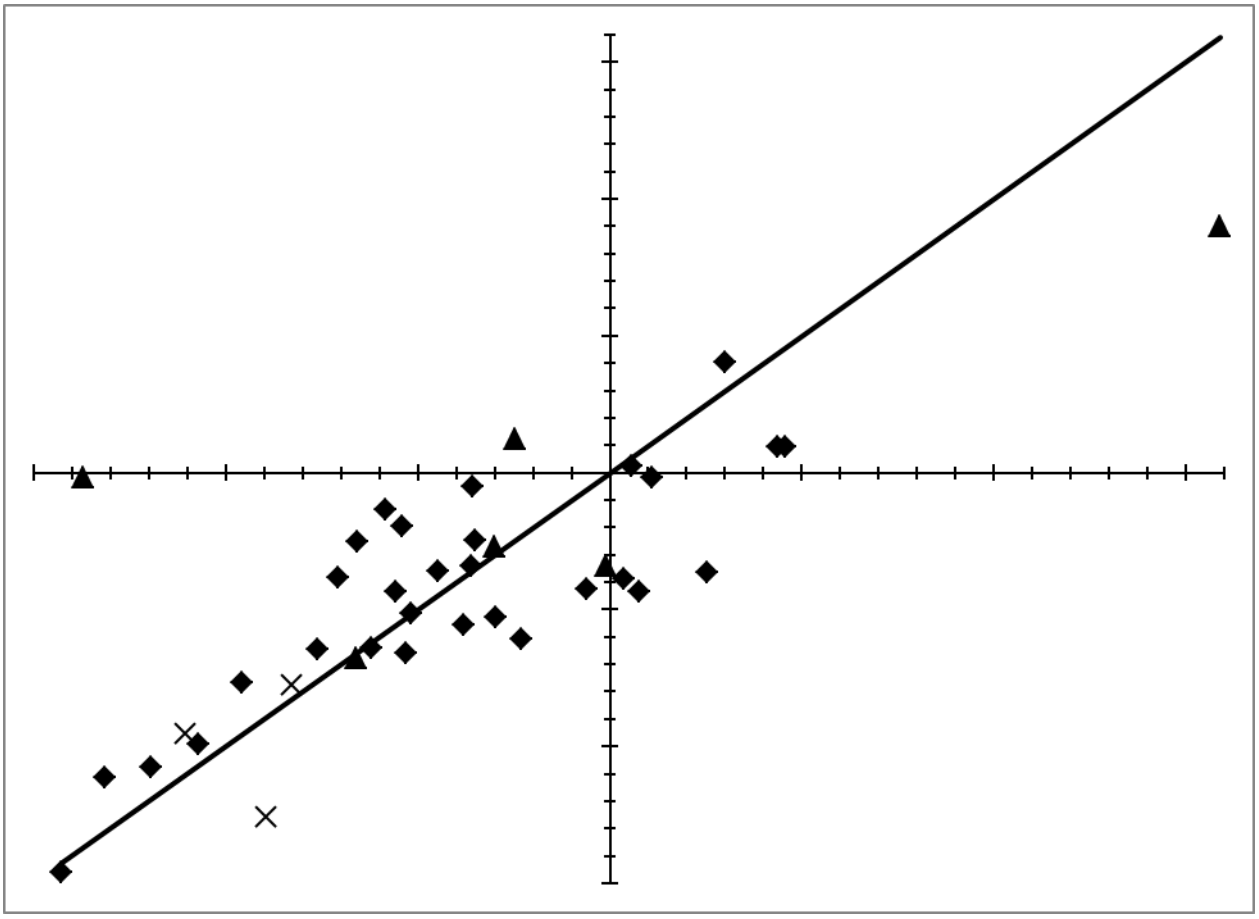

Figure 5. Experimental and L3 regressed values of ln K_{Cl} for our calibration data.

Symbols as in Figure 3.

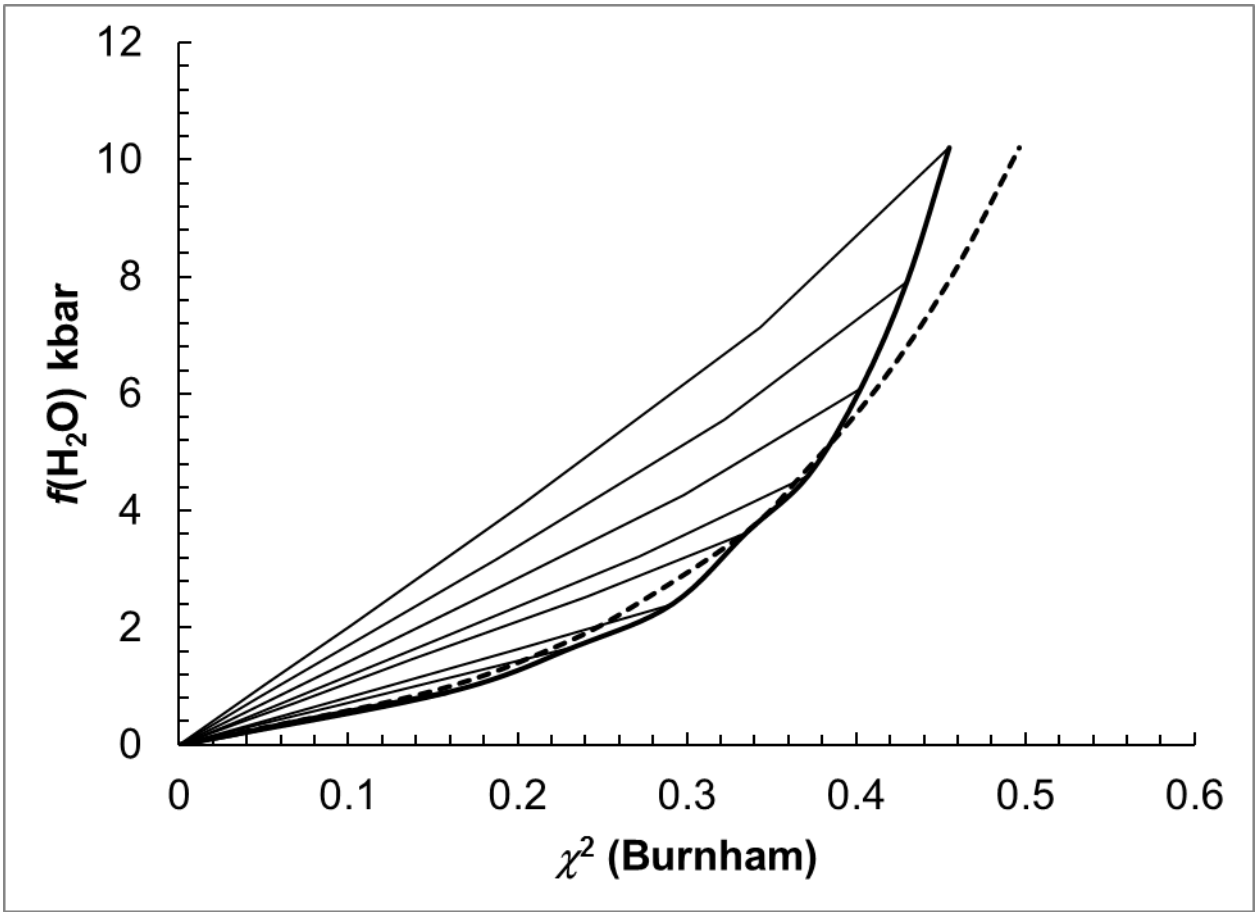

Figure A.1. Moore et al. (1998) solubility curve (dashed line), Burnham (1997) solubility curve (thick solid line), and Burnham undersaturated melt H_2O mole fraction-fugacity lines at 1 to 8 kbar total pressure, 800 °C for the melt composition of synthesis 298 (Sato et al., 2005).